Informatics in Medicine Unlocked 37 (2023) 101162

Contents lists available at ScienceDirect

Informatics in Medicine Unlocked

journal homepage: www.elsevier.com/locate/imu

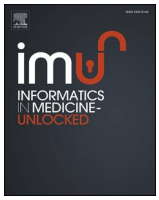

Targeting *Leishmania donovani* sterol methyltransferase for leads using pharmacophore modeling and computational molecular mechanics studies

Patrick O. Sakyi [a,b], Emmanuel Broni [c,d,e], Richard K. Amewu [a,**], Whelton A. Miller III [e,f,g], Michael D. Wilson [d,e], Samuel K. Kwofie [c,h,*]

[a] *Department of Chemistry, School of Physical and Mathematical Sciences, College of Basic and Applied Sciences, University of Ghana, P. O. BOX LG 56, Legon, Accra, Ghana*
[b] *Department of Chemical Sciences, School of Sciences, University of Energy and Natural Resources, Box 214, Sunyani, Ghana*
[c] *Department of Biomedical Engineering, School of Engineering Sciences, College of Basic & Applied Sciences, University of Ghana, Legon, Accra, LG 77, Ghana*
[d] *Department of Parasitology, Noguchi Memorial Institute for Medical Research (NMIMR), College of Health Sciences (CHS), University of Ghana, Legon, Accra, LG 581, Ghana*
[e] *Department of Medicine, Loyola University Medical Center, Maywood, IL, 60153, USA*
[f] *Department of Molecular Pharmacology and Neuroscience, Loyola University Medical Center, Maywood, IL, 60153, USA*
[g] *Department of Chemical and Biomolecular Engineering, School of Engineering and Applied Science, University of Pennsylvania, Philadelphia, PA, 19104, USA*
[h] *Department of Biochemistry, Cell and Molecular Biology, West African Centre for Cell Biology of Infectious Pathogens, College of Basic and Applied Sciences, University of Ghana, P.O. Box LG 54, Accra, Ghana*

ARTICLE INFO

Keywords:
Leishmania donovani
Sterol methyltransferase
Pharmacophore
Ergosterol biosynthesis
Molecular docking
Molecular mechanics

ABSTRACT

The mortalities and morbidities of leishmaniasis are high and the disease is under reported globally. The absence of vaccines coupled with chemotherapeutic challenges including chemoresistance, scarcity and toxicity have made the fight against leishmaniasis an arduous one. Furthermore, the treatment options currently available for leishmaniasis are long and sometimes require hospitalization. There is therefore the need to explore novel pathways to identify new compounds with alternative mechanisms of action. A pharmacophore-based screening was employed in identifying new potential inhibitors with unique scaffolds targeting *Leishmania donovani* sterol methyltransferase (*Ld*SMT), a key enzyme for ergosterol biosynthesis. To accomplish this, 22,26-azasterol, a known inhibitor of this target and five other derivatives with IC_{50} less than 10 μM were used to generate a robust 3D pharmacophore model *via* LigandScout with a score of 0.9144. The validated model was used as a query to screen a library of 69034 natural products obtained from the InterBioScreen Limited. Compounds with pharmacophore fit scores above 50 were docked against the modelled structure of *Ld*SMT. Altogether, ten molecules with binding energies between −7 and −11 kcal/mol were identified as potential bioactive molecules. The molecular dynamics simulation and molecular mechanics Poisson–Boltzmann surface area (MM-PBSA) calculations reinforced the results from the docking studies suggesting the selected hits bind effectively at the active sites of the target protein. The compounds were observed to bind in the S-adenosine-L-homocysteine binding pocket of the modelled *Ld*SMT with Trp208 and Val330 predicted as key residues critical for ligand binding. Prediction of biological activity with probability of activity (Pa) greater than probability of inactivity (Pi) revealed that seven compounds (STOCKIN-54848, STOCKIN-89115, STOCKIN-68720, STOCKIN-44724, STOCKIN-76694, STOCKIN-47277 and STOCKIN-95708) possessed antileishmanial properties. STOCKIN-89115, STOCKIN-68720, STOCKIN-44724, and STOCKIN-47277 were predicted to be membrane permeability inhibitors, while all ten hit compounds possessed antineoplastic activity. The compounds have the propensity of disrupting ergosterol biosynthesis leading to the suppression of growth in *Leishmania donovani*. The compounds were predicted to have good absorption, distribution, metabolism, excretion and toxicity profiles, hence their potential antileishmanial activity can be exploited upon experimental corroboration.

* Corresponding author. Department of Biomedical Engineering, School of Engineering Sciences, College of Basic & Applied Sciences, University of Ghana, Legon, Accra, LG 77, Ghana.
** Corresponding author.
E-mail addresses: opsakyi@st.ug.edu.gh, patrick.sakyi@uenr.edu.gh (P.O. Sakyi), ebroni002@st.ug.edu.gh (E. Broni), ramewu@ug.edu.gh (R.K. Amewu), wmiller6@luc.edu (W.A. Miller), MWilson@noguchi.ug.edu.gh (M.D. Wilson), skkwofie@ug.edu.gh (S.K. Kwofie).

https://doi.org/10.1016/j.imu.2023.101162
Received 7 September 2022; Received in revised form 30 December 2022; Accepted 3 January 2023
Available online 7 January 2023

1. Introduction

Leishmaniasis, caused by over twenty *Leishmania* species and transmitted by more than eighty sandfly species, is second to malaria in terms of mortalities among all the neglected tropical diseases (NTDs) [1]. Visceral leishmaniasis (VL) caused mainly by *L. donovani* and *L. infantum* is the most fatal among the three forms of leishmaniasis and is mostly characterized by irregular bouts of fever, weight loss, enlargement of the liver, and anemia [1,2]. Even more disturbing is the presence of macular, maculopapular, and nodular rash in patients who have undergone successful leishmaniasis treatment [3]. Most of the recovered patients suffer from inferiority complex due to the complications hence struggle to integrate into society because of the ugly scars [4].

VL is endemic in poverty-stricken parts of the world and an estimated 50,000 to 90,000 new cases occur worldwide annually [5]. Most of the cases are recorded in Brazil, Ethiopia, Eritrea, India, Iraq, Kenya, Nepal, Somalia, South Sudan and Sudan [6,7]. Socioeconomic conditions, malnutrition, population mobility, environmental and climate change are the major risk factors associated with this disease [8]. *Leishmania* parasites are transmitted through the bites of infected female phlebotomine sandflies, which feed on blood to produce eggs [9]. The epidemiology of VL is complex and depends on parasite characteristics and sandfly species. Local ecological characteristics of the transmission sites, current and past exposure of the human population and behaviors have contributed to the challenges associated with VL treatments. Moreover, lack of comprehensive understanding of the ergosterol, the main sterol biosynthesized in *Leishmania* parasites and their essentiality for the parasite's survival have also made the treatment of VL a challenging one.

Sterol methyltransferase (SMT), a potential target for the treatment of leishmaniasis, catalyzes the transfer of a methyl group from S-adenosine-methionine to the C24 position of the sterol side chain during ergosterol biosynthesis (Fig. 1) [7]. This target has provided the focus for study of electrophilic alkylations, a reaction type of functional importance that results in the formation of C–C bond in natural products [10]. Inhibitors of SMT have shown antiproliferative effects against pathogenic fungi [11,12], *Trypanosoma cruzi* [13] and *T. brucei* [14,15]. Moreover, 22,26-azasterol, a known SMT inhibitor induces drastic changes in the sterol profile of *L. donovani* and *L. amazonensis* characterized by the loss of ergostane-based sterols and their replacements by 24-desalkyl sterols, along with significant growth reduction and subsequently elimination of the parasite [11]. In addition, SMT inhibitors also cause profound structural changes in the plasma membrane, mitochondrial membrane, and endoplasmic reticulum of *L. amazonensis* [16–18]. The effects of SMT inhibition on parasite's survival coupled with the absence of SMT orthologues in humans makes SMT a potential target for exploitation therapeutically for drug design against *Leishmania* parasites.

There are currently no vaccines for combating VL and all other forms of leishmaniasis as the current drugs used to treat the disease including pentavalent antimony, pentamidine (PTM), amphotericin B (Amp B), miltefosine (Milt), paromomycin and liposomal Amp B are plagued with numerous challenges such as long treatment durations, cytotoxicity, resistance, and high cost [19,20]. Synergistic resistance has also been observed in partner drugs used in combinational chemotherapies. As a result there is the need to find new chemotypes by exploring novel pathways to identify new compounds with alternative mechanisms of action from the existing drugs [7]. In our earlier study, we employed *de novo* design to predict inhibitors against SMT [21]. Pharmacophore-based drug design is an alternative to *de novo* design. This approach though cheaper, has however been employed in rational drug design to overcome most of the challenges associated with drug inefficiencies and resistance [22]. In addition, pharmacophore-based drug design explores diversity thus increases the chance of attaining leads and promotes specificity [23,24] in the design of potent inhibitors against plausible targets. Pharmacophore, an ensemble of steric and electronic features in a molecule recognizable at a protein's binding site and responsible for a molecule's biological activity [22], has been employed in recent strategies for the design of drugs for treatment of cancer (gefitinib), inflammatory diseases (morazone), microbial infections (finafloxacin) and psychotic diseases (phendimetrazine) [25]. Interestingly, most of the pharmacophore-based drugs exhibit multimodality properties which gives an added advantage and hence helps to overcome the parasite's resistance [26]. Though yet to be fully explored for the design of drugs for leishmaniasis treatment, irosustat, avasimibe, topiramate and RWJ-37497 used for cancer treatments targeting two or more biological targets, were designed based on the core aryl *O*-sulfamate pharmacophore [26]. Similarly, linezolid, timolol, merazone and phendimetrazine used as antibiotic, antihypertensive, anti-inflammatory and antipsychotic drugs, respectively were all designed with the morpholine pharmacophore [25].

Natural products from various sources have been explored for the treatments of numerous debilitating diseases affecting humans [27]. Till date, nature has been one of the main sources of drugs and between 1981 and 2014, about 50% of all US FDA drugs have had their source from molecules isolated from natural sources [28]. This notwithstanding, their synthetic accessibility has hampered their use in some instances, but their structural diversity and low toxicity compared to their synthetic counterparts have made them the most preferred choice in the search for new drugs [27]. Exploring key pharmacophores from natural product isolates could provide a possible means of finding suitable druggable candidates for leishmaniasis treatment.

Since the essentiality of SMT to *Leishmania* parasites is no more in doubt and it is suggested as a plausible target, herein, we present the application of ligand-based pharmacophore screening and molecular docking to identify potential inhibitors from natural products with

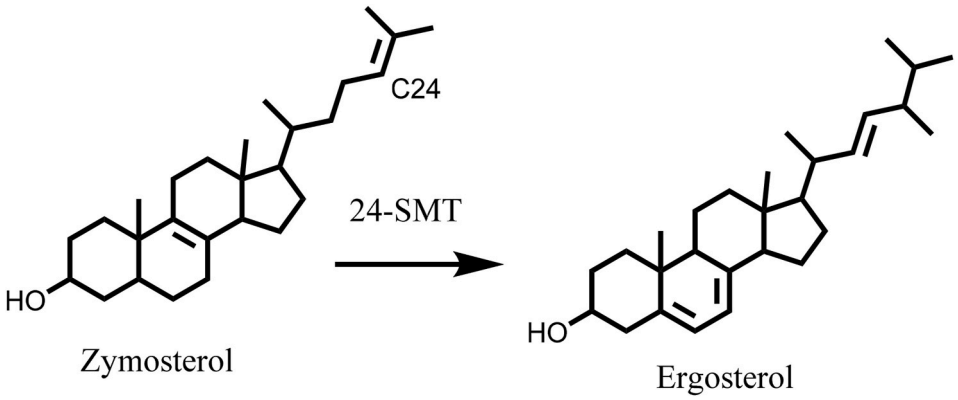

Fig. 1. 24-SMT catalyzes the formation of ergosterol from zymosterol.

unique scaffolds possessing the possibility of ameliorating the activity of *Ld*SMT. The study also seeks to predict the mechanism of binding and biological activity of the proposed compounds.

2. Materials and methods

The scheme (Fig. 2) describes the detailed procedure adopted in the prediction of potential inhibitors from natural products targeting *Ld*SMT. Six ligands including 22,26-azasterol with IC_{50} less than 10 μM were used to generate a pharmacophore model using the merged feature on LigandScout version 4.3 [29]. The pharmacophore model was used to screen a library of natural products from InterBioScreen Limited and ligands with pharmacophore fit scores greater than 50 were subjected to molecular docking studies using a modelled *Ld*SMT structure as the target protein [21]. The potential lead compounds were further evaluated for their physicochemical, pharmacological and toxicity profiles, biological activity predictions and molecular dynamics (MD) computations.

2.1. Protein structure preparation

The modelled 3D structure of *Ld*SMT using Modeller version 10.2 [30] in our previous study [21] was used for this study. The preparation of the protein structure has been previously described [21] and presented here. The 3D *Ld*SMT structure was energy minimized using the Optimized Potentials for Liquid Simulations (OPLS)/All Atom (AA) force filed in GROMACS 2018 [31,32]. Biovia Discovery Studio Visualizer v19.1.0.18287 [33] was used to visualize the energy minimized structure as well as remove water molecules solvating the protein. The structure was then saved in Protein Data Bank (pdb) format using the Biovia Discovery Studio Visualizer v19.1.0.18287 [33]. The structure was then converted to AutoDock Vina's [34] compatible "Protein Data Bank, Partial Charge (Q), & Atom Type (T) (pdbqt)" format for molecular docking.

2.2. Prediction of binding sites

The probable volume and area of the binding site of the modelled protein was determined using the Computed Atlas of Surface Topography of proteins (CASTp) [35], and was described previously [21] and described here. Amino acid residues present in the binding sites were also identified and visualized using Biovia Discovery Studio Visualizer v19.1.0.18287 [33].

2.3. Compound selection for pharmacophore generation

A search through literature identified 22,26-azasterol and its derivatives, imipramine and azetimibe (Table 1) as inhibitors of SMT [17,53,54]. ChemDraw Ultra 12.0 [36] was used to generate the 2D of the chemical structures and Chem3D Pro 12.0 [36] was utilized to generate energy minimized 3D structures. The compound 22,26-azasterol, a known inhibitor of the target protein was specifically docked to the model protein to determine binding mechanisms and consistency within the active site.

2.4. Ligand-based pharmacophore virtual screening

LigandScout version 4.3 [29] was used to generate the pharmacophore model needed for the ligand-based pharmacophore virtual screening. The 3D structures of the SMT inhibitors with IC_{50} less than 10 μM were uploaded onto LigandScout's Ligand-Based Modeling Perspective v4.3 [29] using their Structure Data File (SDF) formats. The default settings of OMEGA best in LigandScout version 4.3 [29] was used in the generation of ligand conformations with 200 conformations being the maximum limit set per molecule.

2.5. Library retrieval and preparation for pharmacophore-based screening

A natural product chemical library from InterBioScreen comprised of 69034 compounds was retrieved [37]. The chemical entities were used for the pharmacophore-based virtual screening.

2.6. Pharmacophore-based virtual screening of the libraries

In all, 69034 chemical entities were used for the pharmacophore screening using LigandScout v.4.3 [29] by first converting from "sdf" to "lbd" before screening against a validated pharmacophore model.

2.7. Validation of both pharmacophore model and AutoDock Vina

Both the pharmacophore model and docking protocol were validated before the virtual screening.

2.7.1. Validation of pharmacophore model

Validation of the pharmacophore model in LigandScout v.4.3 [29] was done using the receiver operating characteristic (ROC) curve and the Enrichment Factor (EF). This was undertaken to ascertain the ability of the pharmacophore model to distinguish between actives and decoys. To do this, the six inhibitors with $IC_{50} < 10$ μM (Table 1) against SMT

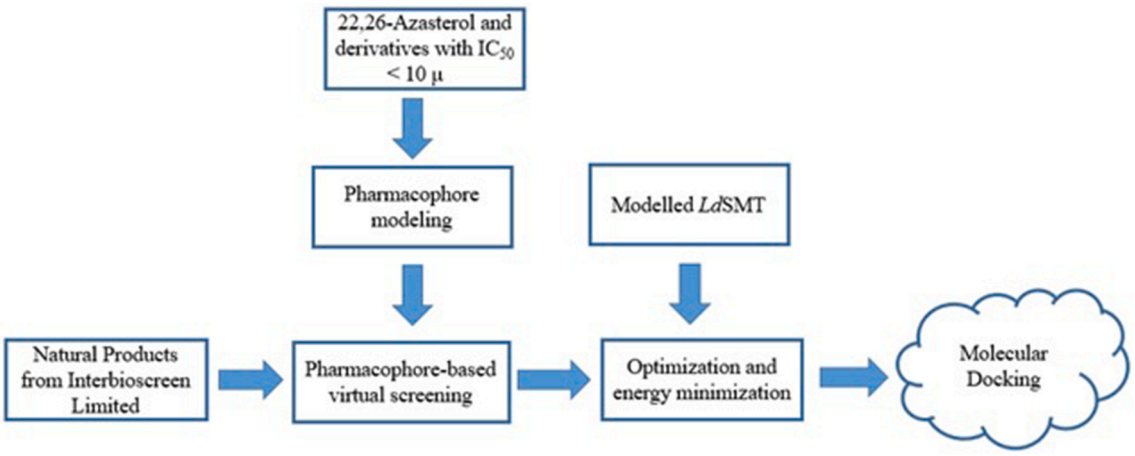

Fig. 2. The workflow employed in predicting potential antileishmanial compounds targeting *Ld*SMT. The scheme provides a pharmacophore-based design coupled with molecular docking and dynamics simulations to identify natural product chemotypes with potential leishmanicidal properties.

Table 1
Chemical structures of six known inhibitors of *Leishmania* parasite sterol methyltransferase and their IC_{50} (μM).

Compound	IC_{50}/μM	Reference
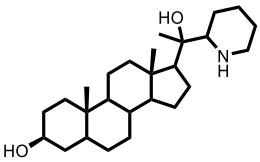 22,26-Azasterol	8.90	[14]
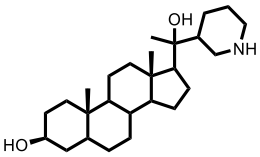 X1	4.80	[14]
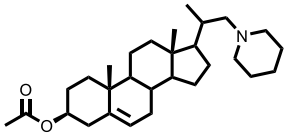 X2	2.50	[14]
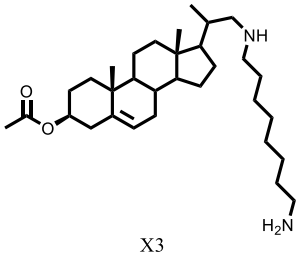 X3	3.85	[14]
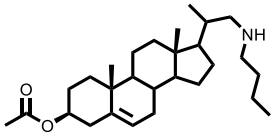 X4	7.70	[14]
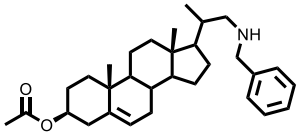 X5	8.90	[14]

and their decoys were used to generate both the ROC curve and EF. The ROC curve is quantified by the calculation of area under the curve (AUC) with values ranging from 0 to 1 and the EF measures the ratio of actives in the top hits of a virtual screen to that expected by random selection, expressed as a percentage [38].

2.7.2. Validation of AutoDock Vina

The six known inhibitors of SMT comprising 22,26-azasterol and its derivatives (Table 1) served as actives for SMT. The SMILES of the six compounds served as inputs for the generation of 50 decoys each *via* Directory of Useful Decoys (DUD-E) [39]. The 306 compounds comprising 6 actives and 300 decoys were docked to the catalytic domain of the *Ld*SMT. EasyROC version 1.3.3 [40] was used to compute the AUC from the ROC curve employing the respective binding energies of the ligands. The calculated AUC was used to validate the ability of AutoDock Vina to differentiate actives from decoys.

2.8. Molecular docking studies of chemical entities with good pharmacophore fit scores

AutoDock Vina [34] interfaced with PyRx v.0.8 [41] was used for the virtual screening as described previously [21]. Ligands with good pharmacophore fit scores obtained after screening the pharmacophore model against the library were imported as spatial data file (sdf) format into AutoDock Vina, energy minimized and converted to pdbqt format. The energy minimization of ligands employed default settings involving universal force field (UFF) and conjugate gradient for optimization algorithm for 200 steps. The energy minimized ligands were then docked against the energy minimized *Ld*SMT using AutoDock Vina [34]. The grid box size was set as previous work [21] to 91.445 × 73.502 × 78.352 $Å^3$ with the center at (72.200, 58.009, 13.302) Å. Ligands were then docked into the binding site of the target protein with exhaustiveness set to 8.

2.9. Characterization of mechanism of binding

The atomistic details of binding between *Ld*SMT and the ligands were determined using the Biovia Discovery Studio Visualizer v19.1.0.18287 [33] as described previously [21].

2.10. ADMET properties and drug-likeness assessment

The absorption, distribution, metabolism, excretion, and toxicity (ADMET) properties of shortlisted compounds were determined using SwissADME [42] and OSIRIS Property Explorer in Data Warrior 5.0.0 [43] for the toxicity effects (mutagenic, tumorigenic, irritant, and reproductive). PAINS and synthetic accessibility were further performed to eliminate false positive compounds that possess good physicochemical properties as well as compounds difficult to synthesize [42].

2.11. Prediction of biological activity of selected compounds

The biological activity of the selected compounds were predicted using the prediction of activity spectra for substances (PASS) [44], which works based on a training dataset of known substances present in its database. The simplified molecular input line entry system (SMILES) files of shortlisted molecules were used as inputs.

2.12. Molecular dynamics simulation and MM-PBSA evaluation of LdSMT-Ligand complexes

The MD simulation and molecular mechanics Poisson–Boltzmann surface area (MM-PBSA) were computed as previously described [21] using GROMACS 2018 [31,32] and g_mmpbsa [45], respectively. The root mean square deviation (RMSD), root mean square fluctuation (RMSF), radius of gyration (Rg) and solvent accessible surface area (SASA) graphs [46] were plotted using Qtgrace [47], while the per-residue energy decomposition graphs were generated using R programming language [48,49].

3. Results and discussion

The results of the pharmacophore modelling, molecular docking, ADMET evaluation, prediction of biological activities of the selected molecules, MD simulations and MM-PBSA calculations are presented.

3.1. Prediction of LdSMT active site residues

Proteins are important class of biological macromolecules which realize their functions by binding to other proteins or small molecules [50]. Understanding protein-ligand interactions is therefore, very essential for studying the biology of the protein at the molecular level and for designing more selective and potent inhibitors against target

proteins [50]. To achieve a better understanding, the binding pocket of a receptor for ligand binding is very crucial. As such, the volume and area of the active site in *Ld*SMT was computed *via* Computed Atlas of Surface Topography of proteins (CASTp) [35]. A binding site volume of 446.632 $Å^3$ and area of 905.262 $Å^2$ were obtained from previous studies [21] with residue positions spanning Gly4, Gly5, Arg6, Glu7, Thr8, Ala30, Arg34, Thr51, Met52, Val53, Asn54, Tyr66, Gly67, Asp108, Val109, Gly110, Cys111, Gly112, Val113, Gly114, Gly115, Pro116, Ala117, Asn132, Gln137, Tyr175, Ala176, Ile177, Glu178, Ala179, Thr180, Cys181, His182, Lys186, Cys189, Tyr190, Val193, Phe203, Leu205, Tyr206, Gly207, Trp208, Met210, Tyr214, Pro216, Asn217, Asp218, Glu219, Tyr220, Arg222, Ile224, Lys225, His226,Arg227, Ile228, Glu229, Leu230, Glu236, Lys241, Met247, Phe252, Ile261, Il269, Ser271, Ile272, Trp274, Tyr275, Leu278, Glu324, Ser328, Leu329, Val330, Val331, Gly332, Gly333 and Leu335 [21].

3.2. Pharmacophore generation

Six of the ligands (Table 1) with IC_{50} less than 10 μM were used to generate the pharmacophore model. Previous studies have used mainly two ligands in generating the pharmacophore model [38,46] but to achieve a significantly robust pharmacophore model, 48 inhibitors were used for generating the model for the design of inhibitors against histone deacetylase 2 (HDAC2) [51]. Similarly, to ensure statistical relevance, a training set containing 18 diverse compounds with experimental activity values (IC_{50}) ranging from 0.5 nM to 5590 nM were employed in the development, evaluation and application of 3D quantitative structural activity relationship (QSAR) pharmacophore model in the discovery of potential human renin inhibitors [52]. In the current study, six compounds (22,26-azasterol and its derivatives) with IC_{50} values less than 10 μM were used as the training set for the generation of a robust and a statistically relevant pharmacophore model. The inherent features of the compounds were identified to generate the hypothetical model. LigandScout [29] allows the generation of 3D pharmacophore model from either the 2D or 3D structural data for any number of ligands compared to other programs which restrict the number of ligands to be used for the model generation. The merge-feature model setting was used in this research instead of the shared-feature because the merge-feature selects all the chemical descriptors present on each ligand even when the descriptors are not common to most of the ligands in the training set [29]. The pharmacophore model generated is scored from 0 to 1 with scores very close to 1 being the most accurate model to distinguish actives from inactives. The generated pharmacophore model was predicted to have a score of 0.9144 based on the merged features from all six ligands and with the score close to 1, it suggests the model can accurately predict actives from the chemical library. The features generated from the pharmacophore modeling consisted of three hydrophobic interactions, one positive ionizable, one hydrogen bond acceptor and one hydrogen bond donor (Fig. 3).

3.3. Validation of pharmacophore model and docking protocol

The ROC curve was employed to validate the pharmacophore model and docking protocol. Six inhibitors of the SMT were used to generate 300 decoys from Database of Useful Decoys: Enhanced (DUD-E) [39], with 50 decoy generated from each ligand. A library comprising six actives and the decoys labelled as "actives" and "inactives", respectively in LigandScout were screened using the best generated pharmacophore model with score 0.9144.

3.3.1. Validation of generated pharmacophore model

A good pharmacophore model should be able to differentiate between actives and inactives (the decoys) from a library of compounds [38]. The ROC measures the performance of the pharmacophore model to effectively differentiate actives from inactives. AUC is assigned values from 0 to 1 with values very close to 1 signifying the model can effectively select actives from a library and 0 meaning incorrect classification [38]. AUC of 0.5 implies poor classification between actives and inactives from a chemical library [38]. The AUC was determined as 1.0, 1.0, 1.0, and 1.0 in the top 1%, 5%, 10% and 100% (Fig. 4) of the screened library, respectively. Altogether, the AUC was observed to be 1.0 implying that the pharmacophore model can efficiently classify

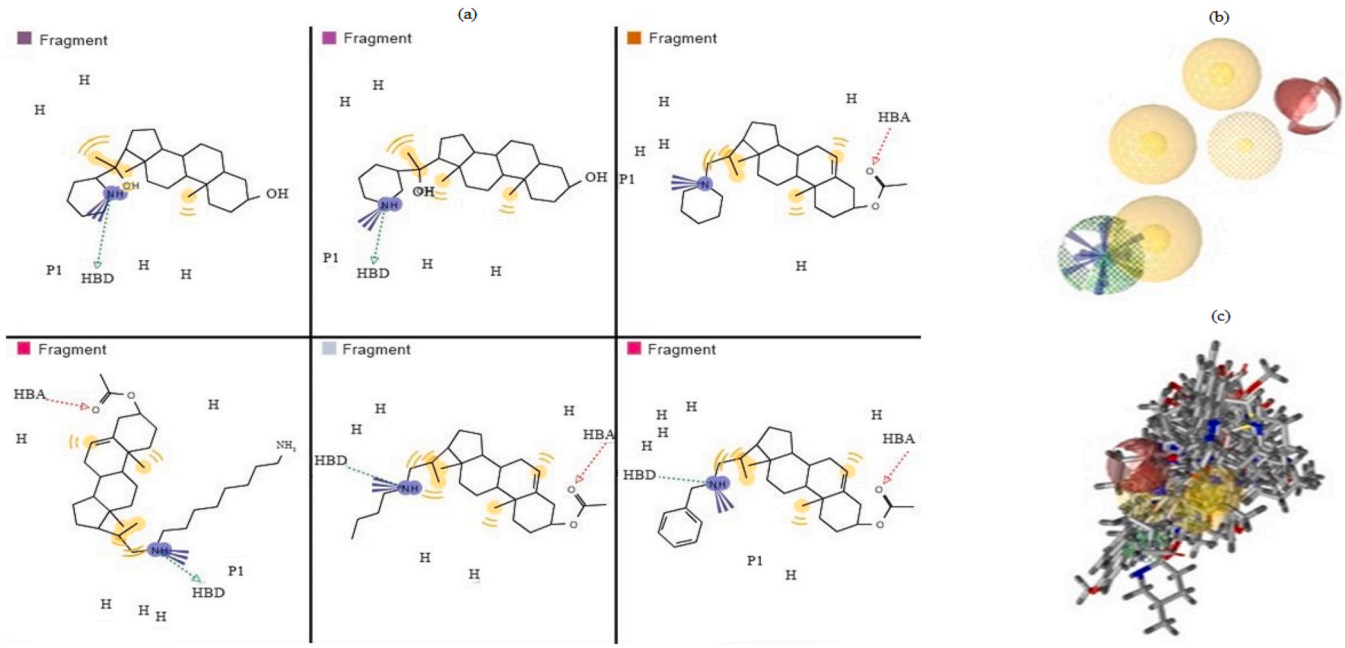

Fig. 3. The pharmacophore features generated from (a) the six ligands comprising hydrophobic interactions (H), positive ionizable (PI), hydrogen bond acceptor (HBA) and hydrogen bond donor (HBD), (b) the pharmacophore model produced from merging the pharmacophore descriptors of all six inhibitors. Red balls showing hydrogen bond acceptors (HBA), yellow balls representing hydrophobic interactions (H), green regions showing hydrogen bond donors (HBD) and blue regions representing positive ionizable (PI), and (c) represents the superimposition of the sixteen selected hits on the generated pharmacophore model showing the various regions they align to the model. (For interpretation of the references to colour in this figure legend, the reader is referred to the Web version of this article.)

actives from the chemical library. The enrichment factors (EFs) were determined as 52.0, 26.0, 26.0 and 26.0 for 1%, 5%, 10% and 100% (Fig. 4), respectively. It supports the efficient classification ability of the model.

3.3.2. Validation of docking protocol

The ROC curve was also used to validate the docking protocol of AutoDock Vina [34] to ensure its ability to discriminate actives from inactives. The computed AUC under the ROC curve ranging from 0 to 1 evaluates the performance of AutoDock Vina in classifying actives from decoys. AUCs close to 1 are considered as perfect and below 0.5 as poor [55,56]. The 6 inhibitors of SMT and their decoys were screened against the *Ld*SMT using AutoDock Vina to generate the ROC curve. The computed AUC under the ROC curve was obtained to be 0.9997 (Fig. 5), classified as perfect [56,57], and this suggests AutoDock Vina reasonably differentiates actives from inactive compounds of *Ld*SMT. A recent *in vitro* study corroborates this result as AutoDock Vina was employed successfully to screen FDA drugs against *Ld*SMT and simeprevir was identified to inhibit *Ld*SMT with an IC_{50} of 51.49 μM [58].

3.3.3. Pharmacophore-based screening of library

The validated pharmacophore model was used as a 3D query to screen the chemical library of 69034 natural product compounds. Compounds were matched and filtered based on the pharmacophore fit score of 50 and above for further analysis as done previously [38]. Compounds with steroidal core or synthetic accessibility more than 6 were also withdrawn from further studies. Steroidal core compounds were removed because they have the potential of causing off-target effects consistent with earlier studies [14,59,60]. In addition, compounds with synthetic accessibility greater than 6 are predicted as difficult to synthesize [61] and hence were also withdrawn. In all, 66 compounds (Supplementary Table 1) had pharmacophore fit scores above 50 and hence were selected for downstream studies. The highest and least pharmacophore fit scores observed were 60.56 and 51.80 for STOCKIN-63567 (Table 2) and STOCKIN-57722, respectively (Supplementary Table 1).

3.4. Molecular docking of hits from pharmacophore screening

The binding energy associated with the docked protein-ligand complex is used to identify potential lead compounds against the target of interest [58,62–64]. The 66 compounds (Supplementary Table 1) obtained from the pharmacophore screening and the known inhibitors, X2 and 22,26-azasterol were docked to the binding site of the *Ld*SMT.

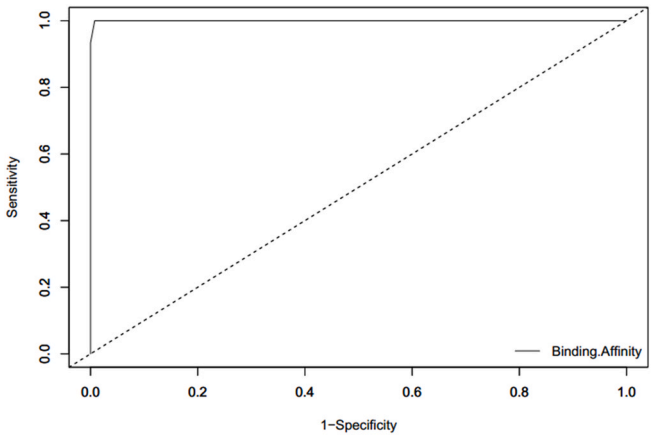

Fig. 5. ROC generated after screening 6 actives and 300 decoys against *Ld*SMT producing an AUC of 0.9997.

The binding energies obtained for the *Ld*SMT-22,26-azasterol and *Ld*SMT-X2 complexes were −7.6 and −7.0 kcal/mol, respectively, similar to previous studies [21]. A potential hit compound should have a binding energy comparable to or lower than that of known inhibitors. Furthermore, the potential hit compound should bind at the active site of the target protein. Similar filtration criteria have already been used in the *in silico* identification of potential inhibitors against plausible targets [65–67]. The 66 compounds were shortlisted to 10, based on compounds whose binding energies were −7.6 kcal/mol or lower, as well as the plausible docking of the ligands at the receptor binding site. Amongst the top 10, STOCKIN-54848 had the least binding energy of −10.1 kcal/mol, while STOCKIN-86259 and STOCKIN-95708 had the highest with both having −7.6 kcal/mol. This suggests the compounds may be good *Ld*SMT binders and may also have the potential of inhibiting *Ld*SMT. STOCKIN-63567 with the highest pharmacophore fit score of 60.56 was eliminated from the downstream analysis since it had a high binding energy of −6.3 kcal/mol indicating a lower binding affinity.

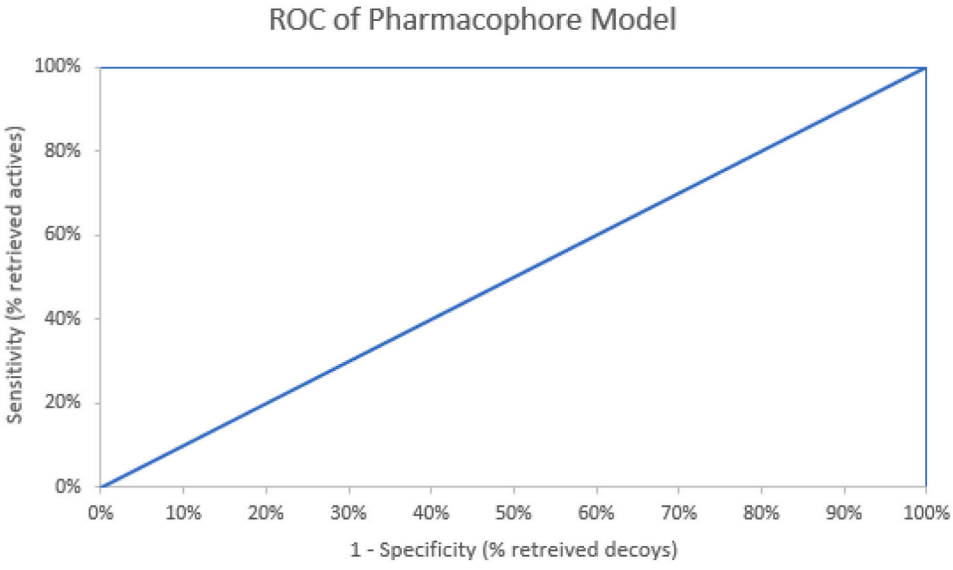

Fig. 4. The ROC of the selected pharmacophore model. The AUCs are 1.0, 1.0, 1.0, and 1.0 in the top 1%, 5%, 10% and 100%, respectively. The EFs at 1%, 5%, 10% and 100% are 52.0, 26.0, 26.0 and 26.0, respectively. The further away of the median (that is, the dotted line) from the curve signifies a good model.

Table 2
The top 20 compounds arranged in order of decreasing pharmacophore fit scores. Downstream analysis was based on all 66 compounds.

Compound ID	Pharmacophore fit score	Binding energy (kcal/mol)	Compound ID	Pharmacophore fit score	Binding energy (kcal/mol)
STOCKIN-63567	60.56	−6.3	STOCKIN-89223	52.96	−7.6
STOCKIN-26015	60.17	−6.1	STOCKIN-58769	52.96	−6.8
STOCKIN-89115	53.98	−8.9	STOCKIN-32756	52.96	−7.1
STOCKIN-88290	53.47	−7.8	STOCKIN-61176	52.90	−8.0
STOCKIN-90413	53.42	−8.6	STOCKIN-92854	52.88	−7.7
STOCKIN-25055	53.35	−6.3	STOCKIN-91725	52.84	−7.1
STOCKIN-86259	53.09	−7.6	STOCKIN-88012	52.82	−7.3
STOCKIN-89039	53.08	−8.2	STOCKIN-40363	52.77	−6.2
STOCKIN-58457	53.07	−7.3	STOCKIN-16871	52.70	−7.7
STOCKIN-95708	53.05	−7.6	STOCKIN-58337	52.59	−7.5

3.5. Protein-ligand interaction

The ligand-protein binding site interaction constitutes the basis of molecular recognition processes [50,68] and it underpins the discovery, design and development of new therapeutic entities [69]. The docking study enables the elucidation of small molecules with high specificity and affinity for the target. All the compounds were observed to dock at the S-adenosine-L-homocysteine (SAH) ligand binding cavity. The examination of all the protein-ligand complexes (Fig. 6, S1a-i, and Table 3) revealed the residues Cys181, Trp208, His226, Ile228, Ile272, Tyr275, and Val330 as critical for binding, similar to an earlier study [21]. The nature of interactions exhibited in all the complexes included *pi*-anion, *pi-pi* stacking, *pi*-alkyl, *pi*-sigma and hydrogen bonding. Out of the 10 selected hits, STOCKIN-54848 formed four hydrogen bonds with active site residues (Fig. 6a) followed by STOCKIN-95708 (Fig. 6b) and STOCKIN-89115 (Fig. 6c), both forming three each with critical residues. STOCKIN-68720, STOCKIN-44724, and STOCKIN-47277 are structurally similar and analogues of chromenone [46]. While STOCKIN-44724 did not form hydrogen bonds with any residue in the binding site of the target protein, compounds STOCKIN-68720 and STOCKIN-47277 on the other hand formed one hydrogen bond each with Glu207 and Val331, respectively (Table 3 and Figs. S1a–c). Hydrophobic profiling revealed that STOCKIN-89115, STOCKIN-68720 and STOCKIN-44724 formed hydrophobic interactions with similar residues including Trp208, Ile228, Leu297, and Val330. Similarly, STOCKIN-89115 and STOCKIN-88290 which are structural derivatives of 2-chromenone [46,70,71] formed hydrogen bonding interactions with Arg295, Thr298, Tyr316 and Glu320. STOCKIN-88290 formed hydrophobic contacts with Arg298, while STOCKIN-89115 formed with Ile296 and Leu297 (Table 3 and Fig. S1e).

STOCKIN-76694 and STOCKIN-19207 formed hydrophobic contacts with Met210, His226, Ile228, and Glu229. STOCKIN-76694 formed a hydrogen bond with Glu229 (Table 3 and Fig. S1f) while STOCKIN-19207 formed one with His226 (Table 3 and Fig. S1d). STOCKIN-95708 formed hydrogen bond interaction with Glu7, Arg227 and Glu236 but STOCKIN-86259 did not form such interaction. However, hydrophobic interactions for STOCKIN-95708 and STOCKIN-86259, included residues Ala9, Leu13, Arg16, Asp218, Ala28, Tyr136, Phe307,His226, Val308, Ala311, and Pro312 (Table 3 and Fig. S1g). STOCKIN-54848 had lower binding energy of −10.1 kcal/mol compared to 22,26-azasterol (7.6 kcal/mol). It formed four hydrogen bonds with critical residues His226, Glu229, Tyr275 and Val331 and formed hydrophobic contacts with Cys181, Lys225 and Ile228 (Table 3 and Fig. 5a) while 22,26-azasterol had hydrophobic interactions with Phe100, Lys198 and Pro199 (Table 3 and Fig. S1i) [21]. One of the known inhibitors of *Ld*SMT, X2 with IC_{50} of 2.5 μM was found not to form hydrogen bonds with any of the amino acids in the binding pocket of the target. However, hydrophobic interactions were formed with

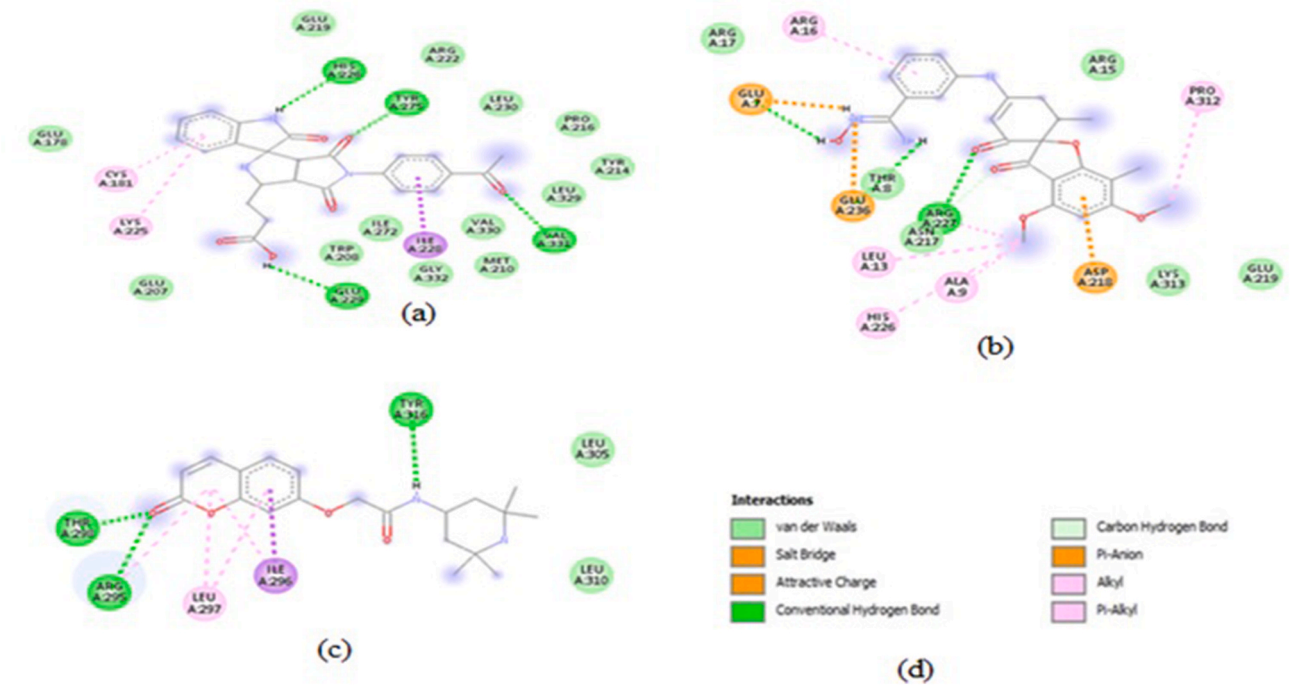

Fig. 6. The 2D interactions of the *Ld*SMT-hits complexes as visualized in Discovery Studio. (a) STOCKIN-54848, (b) STOCKIN-95708, (c) STOCKIN-89115, and (d) legend interactions.

Table 3
Binding energy and predicted binding site residues involved in the *Ld*SMT-ligand complexes formed.

Ligands	Binding Energy/kcal/mol	Binding residues	
		Hydrogen bonds	Hydrophobic bonds
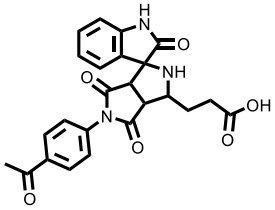 STOCKIN-54848	−10.1	His226, Glu229, Tyr275, Val331	Cys181, Lys225, Ile228
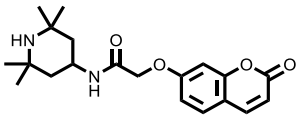 STOCKIN-89115	−8.9	Arg295, Thr298, Tyr316	Ile296, Leu297
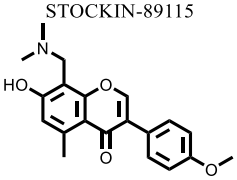 STOCKIN-68720	−8.7	Glu207	Trp208, Ile228, Val330
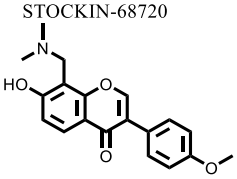 STOCKIN-44724	−8.4		Glu207, Trp208, Ile228, Glu229, Ile272, Val330
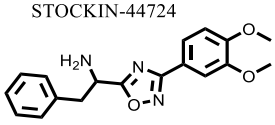 STOCKIN-76694	−8.4	Glu229	Tyr206, Trp208, Met210, Pro216, Ile228, Ser271, Ile272
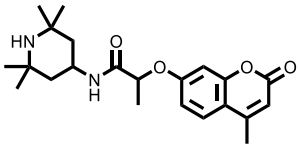 STOCKIN-88290	−7.8	Thr298, Glu320	Arg289
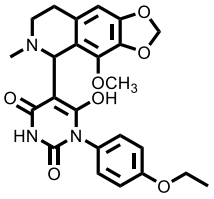 STOCKIN-19207	−7.8	His226	Glu178, Cys181, Met210, Ile228, Glu229
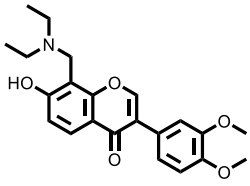 STOCKIN-47277	−7.8	Val331	Trp208, Ile228, Tyr275
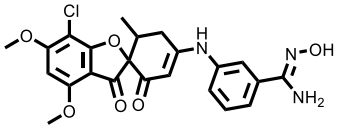 STOCKIN-95708	−7.6	Glu7, Arg227, Glu236	Ala9, Leu13, Arg16, Asp218, His226, Pro312
	−7.6	Arg32, Asp35	Ala28, Tyr136, Phe307, Val308, Ala311

(*continued on next page*)

Table 3 (*continued*)

Ligands	Binding Energy/kcal/mol	Binding residues	
		Hydrogen bonds	Hydrophobic bonds
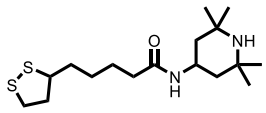 STOCKIN-86259	−7.0		Phe100, Gly200, Cys202, Tyr343, Ile344
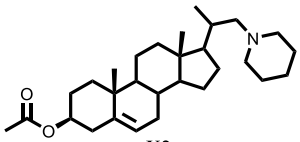 X2	−7.6	Glu102, Gly200	Phe100, Lys198, Pro199
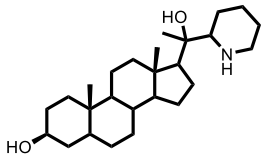 22,26-Azasterol			

residues Phe100, Gly200, Cys202, Tyr343 and Ile344 (Table 3 and Fig. S1h).

3.6. Physicochemical properties of selected molecules

The Lipinski's rule of five (Ro5) was used to determine the physicochemical profiling of the compounds [72,73]. The Ro5 stipulates that for a compound to be orally active then certain parameters must be met which include molecular weight (Mw) ≤ 500 Da, LogP ≤5, hydrogen bond donors ≤5, hydrogen bond acceptors ≤10 and 40 ≤ molar refractivity ≤140 [73]. The Ro5 was used as a criterion for selecting orally active compounds [65]. Similarly, other studies have also used Ro5 in selecting compounds from natural products sources with the potential to be orally active [74–76]. All the 10 selected hit compounds (Table 4) complied with Ro5 and hence predicted to possess good physicochemical properties. The known inhibitors, azetimibe, imipramine, X2 and 22,26-azasterol were also predicted to be orally active since they did not violate any of the Ro5. The Veber's rule suggests compounds can be orally active if the number of rotatable bonds ≤10 and polar surface area ≤140 $Å^2$ [77]. Both the selected hit compounds and known inhibitors were predicted to possess less than 10 rotatable bonds and polar surface areas less than 140 $Å^2$, suggesting their potential as orally active compounds.

Drug solubility is the maximum concentration of the drug that can completely dissolve in a solvent at a constant temperature and pressure and it is evaluated to predict the bioavailability and biological activity of the hit compounds [78]. Recent *in silico* studies employed solubility predictions as criteria for the selection of hit compounds, as many drugs developed have failed clinical trials due to poor solubility [21,67,74]. The identified potential hit compounds (Table 4) were predicted to be soluble suggesting their bioavailability potential. In addition, bioavailability score (BS) which is the fraction of an administered drug that reaches systemic circulation was assessed to differentiate well absorbed compounds from the poor. The selected hit compounds as well as the known inhibitors were predicted to have a bioavailability score of 0.55. A *de novo* design of potential inhibitors of *Ld*SMT identified the novel ligands to possess a bioavailability score of 0.55 [21]. A similar *in silico* study found natural products compounds to have a bioavailability score of 0.55 [74].

Molar refractivity (MR) is the measure of the total polarity of a drug and it is estimated to provide useful information concerning the pharmacokinetics and pharmacodynamics of the molecule [79,80]. The acceptable MR range for drug-like molecules is 40–130 [21]. The predicted hit compounds (Table 4) were all found to have overall polarity within the acceptable range. Similar predictions were observed for 22, 26-azasterol, X2, imipraminn and azetimibe. Synthetic accessibility (SA) is the measure of the overall synthetic feasibility of a molecule and drug-like molecules are predicted to have a synthetic accessibility score lower than 6 [81]. Apart from X2 which showed SA score close to 6 (that is 5.65), the selected inhibitors, 22,26-azasterol, imipramine and

Table 4
Predicted physicochemical and pharmacological profiles of selected compounds and known inhibitors of *Ld*SMT as well as some known drugs for leishmaniasis treatment.

Compounds	Mw (g/mol)	NRB	MR	TPSA ($Å^2$)	LogS	GI	vRo5	BS	SA	BBB	P-gp
STOCKIN-54848	447.44	5	126.78	132.88	−1.26	High	0	0.55	4.51	No	No
STOCKIN-89115	358.43	5	104.73	80.57	−3.56	High	0	0.55	3.29	No	Yes
STOCKIN-68720	339.39	4	98..88	62.91	−4.04	High	0	0.55	3.32	Yes	No
STOCKIN-44724	325.36	4	93.91	62.91	−3.74	High	0	0.55	3.15	Yes	No
STOCKIN-76694	325.36	6	89.69	83.40	−3.64	High	0	0.55	3.69	No	Yes
STOCKIN-88290	386.48	5	98.88	62.91	−4.27	High	0	0.55	3.95	No	Yes
STOCKIN-19207	467.47	5	127.27	115.25	−4.26	High	0	0.55	4.26	No	Yes
STOCKIN-47277	383.44	7	110.02	72.14	−4.28	High	0	0.55	3.62	Yes	No
STOCKIN-95708	471.89	5	121.61	132.47	−5.01	High	0	0.55	4.93	No	Yes
STOCKIN-86259	344.58	7	104.58	91.73	−3.27	High	0	0.55	3.54	No	Yes
Imipramine	280.41	4	93.76	6.48	−4.76	High	0	0.55	2.99	Yes	No
Azetimibe	409.43	6	112.97	60.77	−4.92	High	1	0.55	3.37	Yes	Yes
X2	441.69	5	138.05	29.54	−5.47	High	1	0.55	5.65	No	No
22,26-Azasterol	403..64	2	125.08	52.49	−5.66	High	1	0.55	4.84	Yes	Yes

azetimibe were predicted to possess SA score less than 5 (Table 4). Overall, the selected hit compounds were predicted to be orally active since they conform to the Ro5.

3.7. Pharmacological and toxicity profiling of selected molecules

Pharmacokinetics deals with the movement of a drug in the body [82,83] and its prediction is essential as drug candidates must reach their targets to elicit biological responses [83]. Absorption, distribution, metabolism and excretion (ADME) predictions are employed as criteria for filtering chemical libraries in the identification of hits [46,84]. Some of the key parameters computed herein include gastrointestinal absorption (GI), blood-brain barrier (BBB) and permeability glycoprotein (P-gp). A high GI means the administered drugs can easily be absorbed in the intestines [85]. SwissADME [42] predicted all 10 hit compounds to possess high GI meaning they can easily be absorbed in the intestines and transported to their target receptors. The known inhibitors, X2, imipramine, azetimibe and 22,26-azasterol were also predicted to possess a high GI. Interestingly, an earlier study predicted the anti-leishmanial drugs amphotericin b, paromomycin and miltefosine to show low GI which suggest their low absorption into the blood stream [66]. A drug can cross the brain-barrier to the brain and attach itself to specific receptors to elicit activation of certain signal pathways [86]. Seven of the selected molecules comprising STOCKIN-54848, STOCKIN-89115, STOCKIN-76694, STOCKIN-88290, STOCKIN-19207, STOCKIN-95708 and STOCKIN-86259 (Table 4) were predicted not to cross the brain-barrier. However, STOCKIN-68720, STOCKIN-44714 and STOCKIN-47277 were predicted to have the ability of crossing the BBB. Compared to the known inhibitors, apart from X2 which was predicted not to cross the BBB, the rest comprising imipramine, azetimibe and 22,26 show BBB permeation. A recent study to identify potential leishmanicides targeting cell division cycle (cdc) 2-related kinase 12 (CRK12) shows that five of the selected hit compounds possessed BBB permeation [87]. A drug which is an inhibitor of P-gp will possibly have an increased bioavailability at the site of activity [88]. While STOCKIN-89115, STOCKIN-76694, STOCKIN-88290, STOCKIN-19207, STOCKIN-95708 and STOCKIN-86259 were predicted to be substrates of P-gp, STOCKIN-54848, STOCKIN-68720, STOCKIN-44724 and STOCKIN-47277 were otherwise. On the other hand, four known inhibitors were predicted as P-gp substrates except X2 and imipramine.

The toxicity profiles of the 10 compounds and the known drugs were predicted using OSIRIS Data Warrior 5.0.0 [43]. STOCKIN-54848 and STOCKIN-19207 were predicted to be mutagenic while STOCKIN-54848 and STOCKIN-95708 were predicted as tumorigenic. STOCKIN-88290 and STOCKIN-47277 were predicted to possess reproductive and irritant effects, respectively. This notwithstanding, optimization of the potential hit compounds to generate analogues with improved toxicities can be generated for their effective use in finding a lasting solution for leishmaniasis treatment.

3.8. Biological activity of selected hits

The Open Bayesian machine learning algorithm, Prediction of Activity Spectra for Substances (PASS) [44] was used to predict the biological activity of the selected molecules (Table 5). PASS queries are based on the structure activity relationship (SAR) analysis of the chemical entities present in the database [89].

A total of 7 compounds comprising STOCKIN-54848, STOCKIN-89115, STOCKIN-68720, STOCKIN-44724, STOCKIN-76694, STOCKIN-47277, and STOCKIN-95708 were predicted to possess antileishmanial properties with predicted probability of activity (Pa) values of 0.256, 0.226, 0.391, 0.421, 0.372, 0.479 and 0.380; and probability of inactivity (Pi) values of 0.096, 0.166, 0.052, 0.041, 0.061, 0.027 and 0.057, respectively. The higher Pa values compared to the Pi, suggest the likelihood of these compounds to inhibit the *Ld*SMT and hence worthy of experimental evaluation [90]. In addition, all the compounds were predicted to have antineoplastic effects with Pa greater than Pi. Previous studies have identified a number of anticancer compounds (sunitinib, sorafenib and lapatanib) which have been evaluated against *Leishmania* parasites with some level of successes of which some including bexarotene, imatinib and tamoxifen are already in clinical trials for leishmaniasis treatment [66,91–94].

STOCKIN-89115 and STOCKIN-88290 were predicted to possess dermatological properties with Pa values of 0.196 and 0.244 and Pi values of 0.172 and 0.123, respectively (Table 5) suggesting they can be explored for post kala-azar leishmaniasis [66,95]. STOCKIN-54848, STOCKIN-68720, STOCKIN-44724, STOCKIN-47277 and STOCKIN-86259 were also predicted as 3′-dimethylstaurosporine O-methyltransferase inhibitors with Pa of 0.260, 0.312, 0.28, 0.274 and 0.208; and Pi of 0.081, 0.031, 0.038, 0.04 and 0.104, respectively. In addition, STOCKIN-47277 was predicted as an inhibitor of phenol O-methyltransferase with Pa of 0.23 and Pi of 0.16. Both 3′-dimethylstaurosporine O- methyltransferase and phenol O-methyltransferase belong to the family of transfer of one-carbon group methyltransferases [96–98] of which the target protein, *Ld*SMT is also a member. Therefore, the predicted inhibition of 3′-dimethylstaurosporine O- methyltransferase and phenol O-methyltransferase by the selected hits suggest the compounds to possess the potential of suppressing ergosterol biosynthesis by inhibiting *Ld*SMT. Similarly, these predictions are corroborated by an earlier study which identified potential *Ld*SMT inhibitors *via de novo* design. The identified hits were predicted to suppress 3′-dimethylstaurosporine O- methyltransferase and phenol O- methyltransferase [21]. Furthermore, STOCKIN-89115, STOCKIN-68720, STOCKIN-44724 and STOCKIN-47277 (Table 5) were predicted to be membrane permeability inhibitors with Pa values of 0.394, 0.359, 0.550 and 0.541; and Pi values of 0.206, 0.222, 0.117 and 0.222, respectively. Suramin and other antibiotics (such as fosfomycin, cycloserine, vancomycin and bacitracin) used in treating African trypanosomiasis, cancer and bacterial infections exhibit their mode of action by suppressing membrane permeability [99–101]. This suggests the compounds can be investigated for their ability to inhibit membrane channels and protect

Table 5
Biological activity prediction of selected hits obtained from pharmacophore-based drug design.

Selected Hits	Antileishmanial activities		Antineoplastic activities		Dermatologic		Membrane Permeability Inhibitor	
	Pa	Pi	Pa	Pi	Pa	Pi	Pa	Pi
STOCKIN-54848	0.256	0.096	0.214	0.104	–	–	–	–
STOCKIN-89115	0.226	0.166	0.334	0.133	0.196	0.172	0.394	0.206
STOCKIN-68720	0.391	0.052	0.391	0.108	–	–	0.359	0.222
STOCKIN-44724	0.421	0.041	0.373	0.115	–	–	0.55	0.117
STOCKIN-76694	0.372	0.061	0.286	0.102	–	–	–	–
STOCKIN-88290	–	–	0.349	0.126	0.244	0.123	–	–
STOCKIN-19207	–	–	0.264	0.123	–	–	–	–
STOCKIN-47277	0.479	0.027	0.391	0.108	–	–	0.541	0.124
STOCKIN-95708	0.380	0.057	0.252	0.184	–	–	–	–
STOCKIN-86259	–	–	0.358	0.008	–	–	–	–

cells against toxic and hypotonic stress that will lead to disease exacerbation. Altogether, the selected hits possess novel scaffolds with the potential of inhibiting *Ld*SMT as therapeutic moieties.

3.9. Selection of hits for molecular dynamics simulation

Hit compounds with predicted high Pa pertaining to relevant biological activity require experimental validation [102–105]. STOCKIN-54848, STOCKIN-89115, STOCKIN-68720, STOCKIN-44724, STOCKIN-76694, STOCKIN-47277, and STOCKIN-95708 were predicted to possess anti-leishmanial properties with Pa > Pi. The medicinal properties for chromenone and its derivatives for treatments of various human ailments have been explored [106]. Chromenone scaffolds with promising anti-leishmanial potentials include encecalol angelate which inhibited axenic amastigotes of *L. donovani* at an IC_{50} value of 14.6 μg/mL [70]. The compound 2-(6,8 -Dichloro-2-methyl-4H chromene-4-ylidene) malono nitrile and its analogue, 2-Amino-3-(6,8-dichloro-2-methyl-4H chromen-4-ylidene)prop-1-ene-1,1,3-tricarbonitrile also stopped the growth of intracellular forms at 0.58 and 0.59 μg/mL, respectively [107]. A recent *in silico* studies to find putative hits against *L. major* identified chromen-2-one derivatives as potential inhibitors of *trypanothione reductase* corroborating the earlier *in vitro* and *in vivo* studies [46]. Based on these findings, the selected hits with chromenone moieties including STOCKIN-89115, STOCKIN-68720, STOCKIN-44724, STOCKIN-88290 and STOCKIN-47277 were not considered for MD simulation. The study therefore used potential novel scaffolds (STOCKIN-54848, STOCKIN-76694, STOCKIN-95708) without chromenone backbone together with the known drug (22,26-azasterol) and inhibitor (X2) for the MD simulations. Compound STOCKIN-54848 had four hydrogen bonds coupled with its low binding energy (−10.1 kcal/mol) making it an interesting candidate to investigate further using MD simulation and MM-PBSA calculations.

3.10. Molecular dynamics simulation

A 100 ns MD simulation was performed to check the relative stability of the *Ld*SMT-ligand complexes. The output files were used to generate root mean square deviation (RMSD), root mean square fluctuation (RMSF), and radius of gyration (Rg) plots of the complexes for analysis. The RMSD of the protein backbone of each complex were calculated and plotted against time (Fig. 7a). The RMSD plot explains the fluctuations of the *Ld*SMT protein backbone and evaluates the stability of the protein-ligand complexes [84]. From the RMSD trajectories, it was observed that both the unbound protein as well as complexes of STOCKIN-54848, STOCKIN-76694, STOCKIN-95708, X2 and 22,26-azasterol were equilibrated with RMSD within the range of 0 and 0.6 nm (Fig. 7a), consistent with the *de novo* design of inhibitors against the target [21]. The RMSD of the unbound protein rose from 0 nm to 0.46 nm within a period of 20 ns and then plateaued to the end of the 100 ns simulation. Similar trend was observed for all the other complexes. On comparing the trajectories,

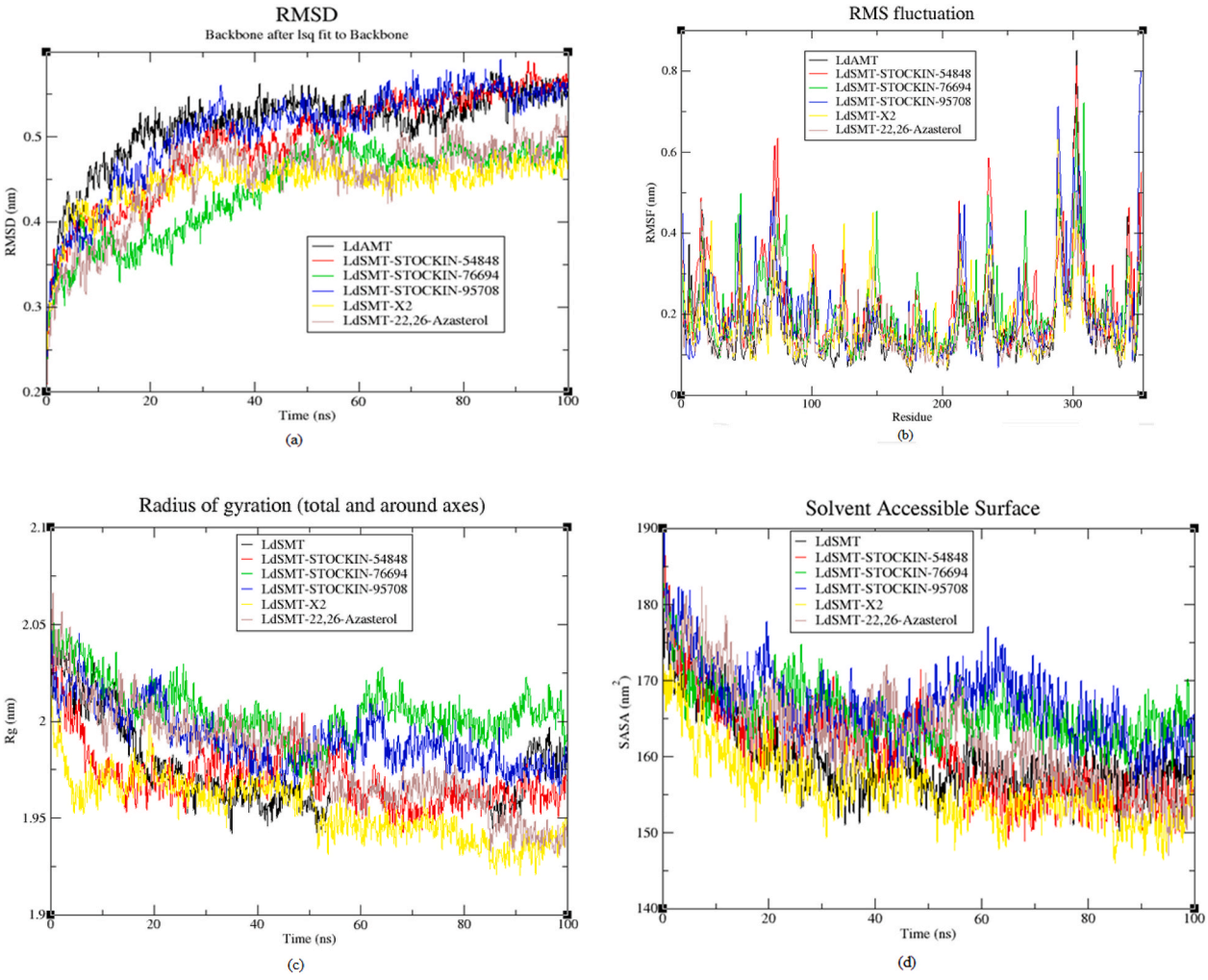

Fig. 7. RMSD, RMSF, Rg and SASA trajectories obtained from the molecular dynamic simulations. (a) RMSD versus time, (b) RMSF versus residue number, and (c) Rg versus time, and (d) SASA versus time for protein-ligand complexes including X2 and 22,26-Azasterol.

the unbound protein trajectory achieved stability with the highest RMSD implying the complexes achieved stability upon equilibration. Among the trajectories of the complexes, both STOCKIN-54848 and STOCKIN-95708 recorded the highest RMSD averaging about 0.2948 and 0.2894 nm, respectively (Table 6) compared to the X2 (0.2515) and 22,26-azasterol (0.2617). Furthermore, STOCKIN-76694 had an average RMSD of 0.2529, lower than 22,26-azasterol but comparable to X2 in terms of stability among the compounds [108].

The amino acid residues in the active site are critical in the stability of protein-ligand complexes [109]. RMSF was used to measure the fluctuations of the amino acid residues to the stability of the complex (Fig. 7b). Amino acid residues between regions 15–100, 200–250, and 280–320 were identified to be critical for the protein-ligand complexes [21]. In this study, amino acid residues within these same regions were found to fluctuate for all the compounds implying that they are critical for binding. This notwithstanding, the highest fluctuation was observed around the region of 280–310 consistent with other studies [21,58,110].

The intermolecular forces of attraction between ligands and proteins determine the rigidness of the complex with a strong force of interaction depicting very compact complex and vice versa [50]. The compactness of the protein-ligand complexes were analyzed by measuring the Rg [66,111]. The Rg trajectory (Fig. 7c) ranging between 1.9 and 2.075 nm suggested the rigidness of the complexes during the entire simulation period. The Rg of the unbound *Ld*SMT declined from 2.05 to about 1.95 nm over a period of 40 ns, then became steady with an average Rg of 1.955 nm until about 80 ns, and then rose steadily to 1.975 nm. The Rg of *Ld*SMT-STOCKIN-54848 complex decreased steadily from 2.04 to about 1.96 nm for 20 ns and then increased slightly to 2.10 nm for 40 ns and then declined steadily thereafter for the next 40 ns. The Rg of *Ld*SMT-STOCKIN-76694 and *Ld*SMT-STOCKIN-95708 complexes experienced similar trends with gradual decline from 2.05 to 1.975 nm over a period of about 50 ns. The Rg values then rose to about 2.025 nm for the next 20 ns and then decreased steadily to an average of 2.0 nm for the last 30 ns. Similar fluctuation trends were observed for *Ld*SMT-X2 and *Ld*SMT-22,26-azasterol complexes with *Ld*SMT-X2 showing the lowest Rg among all the complexes. The average Rg for STOCKIN-54848, STOCKIN-76694, STOCKIN-95708, X2 and 22,26-azasterol complexes were found to be 1.9900, 2.0091, 2.0075, 1.9669 and 1.9992 nm, respectively, consistent with a previous study [21]. This further suggests that X2 formed a stable and rigid complex with *Ld*SMT followed by STOCKIN-54848, 22,26-azasterol, STOCKIN-95708 and STOCKIN-76694. The average Rg value of the five systems was around 1.9945 nm suggesting that all the complexes retained their rigidity throughout the simulations and formed stable complexes with *Ld*SMT.

Moreover, to observe the effects of solvent accessibility occasioned by loose packing on the stability of the protein-ligand complexes, SASA was computed and plotted. The protein-ligand complexes and the unbound protein displayed similar SASA trajectory within the range of 140–190 nm^2 (Fig. 7d) The SASA for the unbound *Ld*SMT decreased from 180 nm^2 to 150 nm^2 within the first 30 ns after which it rose gradually to 160 nm^2 for the next 10 ns and then remained stable thereafter. Similar trajectory was observed for X2 and 22,26-azasterol with stabilization of the trajectory occurring after 30 and 60 ns, respectively during the 100 ns simulation period. However, the complexes of STOCKIN-54848 and STOCKIN-76694 showed an initial decline of SASA in the first 20 ns from 183 to 187 nm^2, respectively to ~160 nm^2 before rising for the next 10 ns. While STOCKIN-76694 stabilized during the remaining 70 ns, the SASA for STOCKIN-54848 decreased to 155 nm^2 and then remained stable for the remaining period of the simulation. On the other hand, the SASA of the STOCKIN-95708 decreased from 180 to 165 nm^2 in the initial 40 ns of the simulation and then rose to 175 nm^2 in the next 20 ns. It decreased again to 155 nm^2 at the 90 ns mark before becoming stable. Comparatively, the average SASA recorded for STOCKIN-54848, STOCKIN-76694, STOCKIN-95708, X2 and 22,26-azasterol are 166.152, 172.178, 171.837, 163.254 and 167.139 nm^2, respectively (Table 6). As a rule of thumb, low SASA values imply limited solvent surface charges resulting in structural restrictions of protein-ligand complexes leading to a more compact and stable configuration [111]. Consequently, considering the average of the computed SASA values for the various complexes, the order of stability is accordingly X2 > STOCKIN-54848 > 22,26-azasterol > STOCKIN-95708 > STOCKIN-76694. The low SASA values recorded for all the complexes signify their stability throughout the 100 ns simulation period.

3.11. MM-PBSA calculations

The MM-PBSA method was used in calculating the free energy of binding (ΔG_{bind}), *van der Waals* interactions energy (ΔG_{vdW}), electrostatic energy (ΔG_{ele}), polar solvation energy ($\Delta G_{pol,\ sol}$) and non-polar solvation energy (ΔG_{SASA}) of the selected protein-ligand complexes [112,113]. A high negative ΔG_{bind} value for each complex except for *Ld*SMT-STOCKIN-95708 complex signifies a strong affinity of the small molecules towards the *Ld*SMT corroborating results from the docking studies [50,114]. The complex of STOCKIN-54848 which was predicted to have the least binding energy (−10.1 kcal/mol) from AutoDock Vina was shown to have free binding energy (−127.838 kJ/mol) lower and comparable to the known inhibitors, 22,26-azasterol (−72.305 kJ/mol) and X2 (−129.725 kJ/mol), respectively. Similarly, STOCKIN-76694 exhibited the lowest free binding energy (−149.899 kJ/mol) among the selected hits as well as X2 and 22,26-azasterol. STOCKIN-95708 showed a high free binding energy of +4190.558 kJ/mol when it had −7.6 kcal/mol obtained from Autodock Vina rendering STOCKIN-95708 not fit to be a hit. This notwithstanding, the main contributor to the free energy of binding was found to be *van der Waal* (ΔG_{vdW}) and is responsible for the embedded hydrophobic binding site of the target protein. The next dominating energy contributor is ΔG_{ele} with values ranging from −94.983 to −3.390 kJ/mol followed by polar solvation energies with −15.475 kJ/mol being the least energy contributed for the complexes (Table 7). The energy contributions suggest that the selected hits except STOCKIN-95708 have more propensity to be potential inhibitors of *Ld*SMT.

Table 6
The maximum, minimum and average RMSD, RMSF and Rg values obtained from MD simulations.

Complex		STOCKIN-54848	STOCKIN-76694	STOCKIN-95708	X2	22,26-Azasterol
RMSD (nm)	Maximum	0.5890	0.5052	0.5783	0.5024	0.5229
	Minimum	0.0005	0.0005	0.0005	0.0005	0.0005
	Average	0.2948	0.2529	0.2894	0.2515	0.2617
RMSF (nm)	Maximum	0.8140	0.7223	0.8001	0.6327	0.5129
	Minimum	0.0818	0.0867	0.0710	0.0685	0.0719
	Average	0.4479	0.4045	0.4355	0.3506	0.2920
Rg (nm)	Maximum	2.0374	2.0508	2.0526	2.0131	2.0662
	Minimum	1.9426	1.9674	1.9623	1.9206	1.9323
	Average	1.9900	2.0091	2.0075	1.9669	1.9992
SASA (nm^2)	Maximum	183.370	187.281	189.524	180.466	187.260
	Minimum	148.934	157.075	154.149	146.042	147.017
	Average	166.152	172.178	171.837	163.254	167.139

The energy contributions of critical amino acid residues are essential for the stability of protein-ligand complexes [38,115]. The per-residue decomposition was employed to determine the energy input of each residue and as a rule of thumb, residues with energies $\geq +5$ kJ/mol or ≤ -5 kJ/mol are regarded as critical for ligand binding [116]. Among the three selected hits, STOCKIN-76694 had residues Trp208, Glu229 and Leu230 (Fig. 8) contributing energies above or below +5 or −5 kJ/mol. The residues Thr8, Pro10, Asn18 and Lys19 (Fig. S2a) were found to provide energies lower than −5 kJ/mol for the stability of the STOCKIN-54848 complex. Compared to the known inhibitors, while none of the residues (Fig. S2b) contributed energies $\geq +5$ kJ/mol or ≤ -5 kJ/mol for the stability of X2, that of Glu102 and Lys198 (Fig. S2c) were critical for the stability of the 22,26-azasterol complex. While the earlier study identified Tyr92 and Ala96 to be critical residues for ligand binding to *Ld*SMT target [21], the current work shows that Thr8, Pro10, Asn18, Lys19, Glu102, Lys198, Trp208, Glu229 and Leu230 amino acids within the binding site also contribute plausible energies required for the stability of the protein-ligand complexes.

4. Future outlook

Pharmacophore-based drug design with its added advantage of incorporating diversity of features and promoting specificity plays pivotal role in the identification of novel chemotypes for different protein targets [67,117–119]. Integration of the predictions with experimental validation will ensure a better means of evaluating the structure, function and modulation of essential therapeutic targets needed to accelerate the drug design pipeline [119–121]. Therefore, the predicted hits in this study could be validated by the efficient and reliable experimented assay to confirm their potential as lead molecules. Mechanisms of binding of the identified hits could be elucidated *via* thermal melt assays [122] followed by evaluation of the physiological activities [123] against the *Leishmania* parasite. Furthermore, a good understanding of the inhibitory effect of the hit molecules would be achieved by performing experimental studies comprising the kinetic and thermodynamic studies [124] of the protein-hit residence time.

The recent upsurge in the interest of the concept of computer-aided drug design (CADD) is attributed to the shortened duration, higher selectivity and reduction in the cost of drug design compared to the traditional means of drug design and development [125]. Some drugs currently in use such as saquinavir, a drug for the treatment of AIDS targeting proteases of HIV 1 and HIV 2, captopril for treating high blood pressure by inhibiting the conversion of angiotensin-converting enzyme and zanamivir which target neuraminidase for influenza A and B treatments were designed by CADD [126]. An *in silico* study identified rutin, a flavonol known for its antioxidant, anticarcinogenic and cardioprotective activities to possess antileishmanial properties targeting *Leishmania donovani* 3-mercaptopyruvate sulfurtransferase [127,128]. *In vitro* studies carried out shows that rutin inhibits *Leishmania donovani* promastigotes and amastigotes with an IC_{50} of 40.95 and 90.09 μM, respectively [128]. Similarly, an *in silico* study identified bisindolylmaleimide IX (BIM IX) to possess multitargeting potential for the treatment of SARS-CoV-2 [63]. *In vitro* studies validated the docking results with IC_{50} of 28.18 μM targeting 3CLpro [63]. Based on the aforementioned, biological activity and cytotoxicity testing *via in vitro* and *in vivo* analysis can be carried out on the identified potential hits to assess their antileishmanial potentials.

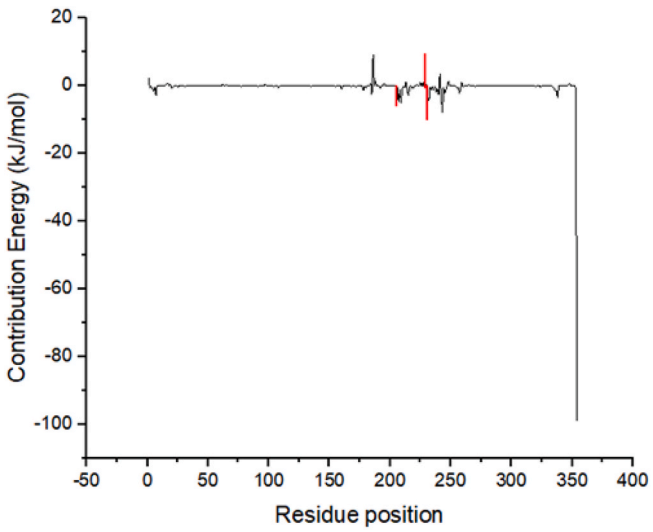

Fig. 8. Per-residue energy decomposition trajectory for the *Ld*SMT-**STOCKIN-76694** complex.

Furthermore, the coordination of the predicted compounds with transition metals targeting sterol methyltransferase could provide a plausible means of combating leishmaniasis.

5. Conclusion

The present work employed pharmacophore-based design, molecular docking and dynamics simulations studies to predict hits with unique scaffolds as potential inhibitors of *Ld*SMT for leishmaniasis treatment. In all, 10 compounds were predicted as potential inhibitors of *Leishmania* parasites attenuating *Ld*SMT with binding energies between −7.6 and −10.1 kcal/mol, which were lower or comparable to the known inhibitor, 22,26-azasterol. MD simulations and MM-PBSA corroborated the docking results with Trp208 and Val330 identified as novel residues critical for ligand binding. While all the compounds were predicted to possess antineoplastic properties, seven of the hits (STOCKIN-54848, STOCKIN-89115, STOCKIN-68720, STOCKIN-44724, STOCKIN-76694, STOCKIN-47277 and STOCKIN-95708) were also predicted to exhibit antileishmanial effects. The bioactivity predictions, pharmacological profiles, binding energies, and binding mechanisms suggest these hits as potential inhibitors of the target protein which need experimental validation to confirm their antileishmanial activity.

Authors' contributions: conceptualization of the project

The project idea was born by P.O.S., S.K.K. and R.K.A. P.O.S. designed the project and executed all the computational analysis with insightful contributions from S.K.K, R.K.A., E.B., W.A.M., and M.D.W. All the authors made their inputs and was accepted by all after P.O.S wrote the first draft before manuscript submission.

Table 7
MM-PBSA free binding energy assessment scores of selected molecules.

Complex	ΔG_{vdW} (kJ/mol)	ΔG_{ele} (kJ/mol)	$\Delta G_{pol,sol}$ (kJ/mol)	ΔG_{SASA} (kJ/mol)	ΔG_{bind} (kJ/mol)
STOCKIN-54848	−181.010 ± 17.506	−94.983 ± 26.865	162.483 ± 37.132	−14.329 ± 2.329	−127.838 ± 25.330
STOCKIN-76694	−217.243 ± 85.589	−6.439 ± 10.576	90.570 ± 47.465	−16.786 ± 6.646	−149.899 ± 58.600
STOCKIN-95708	4135.241 ± 1670.883	−43.493 ± 19.307	118.716 ± 47.409	−19.905 ± 8.383	4190.558 ± 1688.261
X2	−142.275 ± 50.679	−3.390 ± 6.417	29.163 ± 21.101	−13.223 ± 4.385	−129.725 ± 51.799
22,26-Azasterol	−0.047 ± 0.042	−56.829 ± 37.192	−15.475 ± 37.519	0.045 ± 2.716	−72.305 ± 59.057

Funding

This research received no external funding

Institutional review board statement

Not applicable.

Informed consent statement

Not applicable.

Declaration of competing interest

The authors declare that they have no known competing financial interests or personal relationships that could have appeared to influence the work reported in this paper.

Acknowledgments

The authors are grateful to Ghana National Petroleum Corporation (GNPC) for the scholarship awarded Patrick Opare Sakyi for his PhD studies. We also acknowledge West African Centre for Cell Biology of Infectious Pathogens (WACCBIP), University of Ghana for granting free access to Zuputo, a DELL high performance computing system which helped immensely to the successful completion of this work.

Appendix A. Supplementary data

Supplementary data to this article can be found online at https://doi.org/10.1016/j.imu.2023.101162.

References

[1] Jones CM, Welburn SC. Leishmaniasis beyond East Africa. Front Vet Sci 2021;8:618766/1-618766/11. https://doi.org/10.3389/FVETS.2021.618766/BIBTEX.
[2] Ready PD. Epidemiology of visceral leishmaniasis. Clin Epidemiol 2014;6:147–54. https://doi.org/10.2147/CLEP.S44267.
[3] Celesia BM, Cacopardo B, Massimino D, Gussio M, Tosto S, Nunnari G, Pinzone MR. Atypical presentation of PKDL due to leishmania infantum in an HIV-infected patient with relapsing visceral leishmaniasis. Case Rep. Infect. Dis. 2014;2014:1–3. https://doi.org/10.1155/2014/370286.
[4] Bilgic-Temel A, Murrell DF, Uzun S. Cutaneous leishmaniasis: a neglected disfiguring disease for women. Int. J. Women's Dermatology. 2019;5:158–65. https://doi.org/10.1016/J.IJWD.2019.01.002.
[5] Okwor I, Uzonna J. Social and economic burden of human leishmaniasis. Am J Trop Med Hyg 2016;94:489–93. https://doi.org/10.4269/ajtmh.15-0408.
[6] Leta S, Dao THT, Mesele F, Alemayehu G. Visceral leishmaniasis in Ethiopia: an evolving disease. PLoS Neglected Trop Dis 2014;8:e3131/1-e3131/7. https://doi.org/10.1371/journal.pntd.0003131.
[7] Sakyi PO, Amewu RK, Devine RNOA, Bienibuor AK, Miller WA, Kwofie SK. Unravelling the myth surrounding sterol biosynthesis as plausible target for drug design against leishmaniasis. J Parasit Dis 2021;45:1152–71. https://doi.org/10.1007/S12639-021-01390-1.
[8] Hong A, Zampieri RA, Shaw JJ, Floeter-Winter LM, Laranjeira-Silva MF. One health approach to Leishmaniases: understanding the disease dynamics through diagnostic tools. Pathogens 2020;9(2020):809–33. https://doi.org/10.3390/PATHOGENS9100809. Vol. 9, Page 809.
[9] Rogers ME, Bates PA. Leishmania manipulation of sand fly feeding behavior results in enhanced transmission. PLoS Pathog 2007;3. https://doi.org/10.1371/JOURNAL.PPAT.0030091. 0818–0825.
[10] Nes WD. Sterol methyl transferase: enzymology and inhibition. Biochim Biophys Acta, Mol Cell Biol Lipids 2000;1529:63–88. https://doi.org/10.1016/S1388-1981(00)00138-4.
[11] Mukherjee S, Xu W, Hsu FF, Patel J, Huang J, Zhang K. Sterol methyltransferase is required for optimal mitochondrial function and virulence in Leishmania major. Mol Microbiol 2019;111:65–81. https://doi.org/10.1111/mmi.14139.
[12] Urbina JA, Vivas J, Visbal G, Contreras LM. Modification of the sterol composition of Trypanosoma (Schizotrypanum) cruzi epimastigotes by Δ24(25)-sterol methyl transferase inhibitors and their combinations with ketoconazole. Mol Biochem Parasitol 1995;73:199–210. https://doi.org/10.1016/0166-6851(95)00117-j.
[13] Reigada C, Sayé M, Valera-Vera E, Miranda MR, Pereira CA. Repurposing of terconazole as an anti Trypanosoma cruzi agent. Heliyon 2019;5:e01947/1-e01947/5. https://doi.org/10.1016/J.HELIYON.2019.E01947.
[14] Lorente SO, Rodrigues JCF, Jiménez CJ, Joyce-Menekse M, Rodrigues C, Croft SL, Yardley V, De Luca-Fradley K, Ruiz-Pérez LM, Urbina J, De Souza W, González Pacanowska D, Gilbert IH. Novel azasterols as potential agents for treatment of leishmaniasis and trypanosomiasis. Antimicrob Agents Chemother 2004;48:2937–50. https://doi.org/10.1128/AAC.48.8.2937-2950.2004.
[15] Gros L, Castillo-Acosta VM, Jiménez CJ, Sealey-Cardona M, Vargas S, Estévez AM, Yardley V, Rattray L, Croft SL, Ruiz-Perez LM, Urbina JA, Gilbert IH, González-Pacanowska D. New azasterols against Trypanosoma brucei: role of 24-sterol methyltransferase in inhibitor action. Antimicrob Agents Chemother 2006;50:2595–601. https://doi.org/10.1128/AAC.01508-05.
[16] Rodrigues JCF, Attias M, Rodriguez C, Urbina JA, De Souza W. Ultrastructural and biochemical alterations induced by 22,26-azasterol, a Δ24(25)-sterol methyltransferase inhibitor, on promastigote and amastigote forms of Leishmania amazonensis. Antimicrob Agents Chemother 2002;46:487–99. https://doi.org/10.1128/AAC.46.2.487-499.2002.
[17] Magaraci F, Jimenez Jimenez C, Rodrigues C, Rodrigues JCF, Vianna Braga M, Yardley V, De Luca-Fradley K, Croft SL, De Souza W, Ruiz-Perez LM, Urbina J, Gonzalez Pacanowska D, Gilbert IH. Azasterols as inhibitors of sterol 24-methyltransferase in leishmania species and trypanosoma cruzi. J Med Chem 2003;46:4714–27. https://doi.org/10.1021/jm021114j.
[18] Rodrigues JCF, Bernardes CF, Visbal G, Urbina JA, Vercesi AE, de Souza W. Sterol methenyl transferase inhibitors alter the ultrastructure and function of the leishmania amazonensis mitochondrion leading to potent growth inhibition. Protist 2007;158:447–56. https://doi.org/10.1016/j.protis.2007.05.004.
[19] Sakyi PO, Amewu RK, Devine RNOA, Ismaila E, Miller WA, Kwofie SK. The search for putative hits in combating leishmaniasis: the contributions of natural products over the last decade. Nat Products Bioprospect 2021;11:489–544. https://doi.org/10.1007/S13659-021-00311-2.
[20] Ghorbani M, Farhoudi R. Leishmaniasis in humans: drug or vaccine therapy? Drug Des Dev Ther 2018;12:25. https://doi.org/10.2147/DDDT.S146521.
[21] Sakyi PO, Broni E, Amewu RK, Miller WAI, Wilson MD, Kwofie SK. Homology modeling, de Novo design of ligands, and molecular docking identify potential inhibitors of leishmania donovani 24-sterol methyltransferase. Front Cell Infect Microbiol 2022:657. https://doi.org/10.3389/FCIMB.2022.859981. 0.
[22] Qing X, Lee XY, De Raeymaeker J, Tame JR, Zhang KY, De Maeyer M, Voet AR. Pharmacophore modeling: advances, limitations, and current utility in drug discovery. J Recept Ligand Channel Res 2014;7:81–92. https://doi.org/10.2147/JRLCR.S46843.
[23] Kaserer T, Beck KR, Akram M, Odermatt A, Schuster D, Willett P. Pharmacophore models and pharmacophore-based virtual screening: concepts and applications exemplified on hydroxysteroid dehydrogenases. Molecules 2015;20:22799–832. https://doi.org/10.3390/molecules201219880.
[24] Pandit D, So SS, Sun H. Enhancing specificity and sensitivity of pharmacophore-based virtual screening by incorporating chemical and shape features - a case study of HIV protease inhibitors. J Chem Inf Model 2006;46:1236–44. https://doi.org/10.1021/CI050511A.
[25] Kumari A, Singh RK. Morpholine as ubiquitous pharmacophore in medicinal chemistry: deep insight into the structure-activity relationship (SAR). Bioorg Chem 2020;96:103578/1-103578/78. https://doi.org/10.1016/J.BIOORG.2020.103578.
[26] Thomas MP, Potter BVL. Discovery and development of the aryl O-sulfamate pharmacophore for oncology and womens health. J Med Chem 2015;58:7634–58. https://doi.org/10.1021/ACS.JMEDCHEM.5B00386.
[27] Amewu RK, Sakyi PO, Osei-safo D. Synthetic and naturally occurring heterocyclic anticancer compounds with multiple biological targets. Molecules 2021;26:7134/1-7134/48.
[28] Newman DJ, Cragg GM. Natural products as sources of new drugs from 1981 to 2014. J Nat Prod 2016;79:629–61. https://doi.org/10.1021/ACS.JNATPROD.5B01055.
[29] Wolber G, Langer T. LigandScout: 3-D pharmacophores derived from protein-bound ligands and their use as virtual screening filters. J Chem Inf Model 2005;45:160–9. https://doi.org/10.1021/CI049885E.
[30] Eswar N, Eramian D, Webb B, Shen MY, Sali A. Protein structure modeling with MODELLER. Methods Mol Biol 2008;426:145–59. https://doi.org/10.1007/978-1-60327-058-8_8.
[31] Van Der Spoel D, Lindahl E, Hess B, Groenhof G, Mark AE, Berendsen HJC. GROMACS: fast, flexible, and free. J Comput Chem 2005;26:1701–18. https://doi.org/10.1002/JCC.20291.
[32] Abraham MJ, Murtola T, Schulz R, Páll S, Smith JC, Hess B, Lindah E. Gromacs: high performance molecular simulations through multi-level parallelism from laptops to supercomputers. SoftwareX 2015;1:19–25. https://doi.org/10.1016/J.SOFTX.2015.06.001.
[33] Šudomová M, Hassan STS, Khan H, Rasekhian M, Nabavi SM. A multi-biochemical and in silico study on anti-enzymatic actions of pyroglutamic acid against PDE-5, ACE, and urease using various analytical techniques: unexplored pharmacological properties and cytotoxicity evaluation. Biomolecules 2019;9:392–405. https://doi.org/10.3390/BIOM9090392.
[34] Trott O, Olson AJ, Vina AutoDock. Improving the speed and accuracy of docking with a new scoring function, efficient optimization and multithreading. J Comput Chem 2010;31:455–61. https://doi.org/10.1002/JCC.21334.
[35] Tian W, Chen C, Lei X, Zhao J, Liang J. CASTp 3.0: computed atlas of surface topography of proteins. Nucleic Acids Res 2018;46:W363. https://doi.org/10.1093/nar/gky473. –W367.
[36] Kerwin SM. ChemBioOffice Ultra 2010 suite. J Am Chem Soc 2010;132:2466–7. https://doi.org/10.1021/JA1005306.

[37] Sorokina M, Steinbeck C. Review on natural products databases: where to find data in 2020. J Cheminf 2020;12:1–51. https://doi.org/10.1186/S13321-020-00424-9.
[38] Kwofie SK, Dolling NNO, Donkoh E, Laryea GM, Mosi L, Miller WA, Adinortey MB, Wilson MD. Pharmacophore-guided identification of natural products as potential inhibitors of mycobacterium ulcerans cystathionine γ-synthase metb. Computation 2021;9:1–24. https://doi.org/10.3390/computation9030032.
[39] Mysinger MM, Carchia M, Irwin JJ, Shoichet BK. Directory of useful decoys, enhanced (DUD-E): better ligands and decoys for better benchmarking. J Med Chem 2012;55:6582–94. https://doi.org/10.1021/jm300687e.
[40] Goksuluk D, Korkmaz S, Zararsiz G, Karaagaoglu AE. easyROC: an interactive web-tool for ROC curve analysis using R language environment. R J 2016;8:213–30.
[41] Dallakyan S, Olson AJ. Small-molecule library screening by docking with PyRx. Methods Mol Biol 2015;1263:243–50. https://doi.org/10.1007/978-1-4939-2269-7_19.
[42] Daina A, Michielin O, Zoete V. SwissADME: a free web tool to evaluate pharmacokinetics, drug-likeness and medicinal chemistry friendliness of small molecules. Sci Rep 2017;7:42717/1-42717/13. https://doi.org/10.1038/SREP42717.
[43] Sander T, Freyss J, Von Korff M, Rufener C. DataWarrior: an open-source program for chemistry aware data visualization and analysis. J Chem Inf Model 2015;55:460–73. https://doi.org/10.1021/CI500588J.
[44] Lagunin A, Stepanchikova A, Filimonov D, Poroikov V. PASS: prediction of activity spectra for biologically active substances. Bioinformatics 2000;16:747–8. https://doi.org/10.1093/BIOINFORMATICS/16.8.747.
[45] Kumari R, Kumar R, Lynn A. g_mmpbsa —a GROMACS tool for high-throughput MM-PBSA calculations. J Chem Inf Model 2014;54:1951–62. https://doi.org/10.1021/ci500020m.
[46] Kwofie SK, Kwarko GB, Broni E, Adinortey MB, Wilson MD. Molecular informatics of trypanothione reductase of Leishmania major reveals novel chromen-2-one analogues as potential leishmanicides. 2021, 100594/1-100594/36. https://doi.org/10.5772/INTECHOPEN.100594. IntechOpen.
[47] Dahiya R, Mohammad T, Gupta P, Haque A, Alajmi MF, Hussain A, Hassan MI. Molecular interaction studies on ellagic acid for its anticancer potential targeting pyruvate dehydrogenase kinase 3. RSC Adv 2019;9:23302–15. https://doi.org/10.1039/C9RA02864A.
[48] Tippmann S. Programming tools: adventures with R. Nature 2014;517:109–10. https://doi.org/10.1038/517109a.
[49] Alkarkhi AFM, Alqaraghuli WAA. R statistical software. Appl Stat Environ Sci R 2020;1:1–17. https://doi.org/10.1016/b978-0-12-818622-0.00002-2.
[50] Du X, Li Y, Xia YL, Ai SM, Liang J, Sang P, Ji XL, Liu SQ. Insights into protein–ligand interactions: mechanisms, models, and methods. Int J Mol Sci 2016;17:144/1-144/34. https://doi.org/10.3390/IJMS17020144.
[51] Kandakatla N, Ramakrishnan G. Ligand based pharmacophore modeling and virtual screening studies to design novel HDAC2 inhibitors. Adv Bioinformatics 2014;2014:1–11. https://doi.org/10.1155/2014/812148.
[52] John S, Thangapandian S, Arooj M, Hong JC, Kim KD, Lee KW. Development, evaluation and application of 3D QSAR Pharmacophore model in the discovery of potential human renin inhibitors. BMC Bioinf 2011;12:1–14. https://doi.org/10.1186/1471-2105-12-S14-S4/FIGURES/9.
[53] Andrade-Neto VV, Pereira TM, do Canto-Cavalheiro M, Torres-Santos EC. Imipramine alters the sterol profile in Leishmania amazonensis and increases its sensitivity to miconazole. Parasites Vectors 2016;91(9):1–8. https://doi.org/10.1186/S13071-016-1467-8. 2016.
[54] Torres-Santos EC, Andrade-Neto VV, Cunha-Júnior EF, Do Canto-Cavalheiro MM, Atella GC, De Almeida Fernandes T, Costa PRR. Antileishmanial activity of ezetimibe: inhibition of sterol biosynthesis, in vitro synergy with azoles, and efficacy in experimental cutaneous leishmaniasis. Antimicrob Agents Chemother 2016;60:6844–52. https://doi.org/10.1128/AAC.01545-16.
[55] Empereur-Mot C, Guillemain H, Latouche A, Zagury JF, Viallon V, Montes M. Predictiveness curves in virtual screening. J Cheminf 2015;7:1–17. https://doi.org/10.1186/S13321-015-0100-8/TABLES/4.
[56] Mandrekar JN. Receiver operating characteristic curve in diagnostic test assessment. J Thorac Oncol 2010;5:1315–6. https://doi.org/10.1097/JTO.0B013E3181EC173D.
[57] Hsin KY, Matsuoka Y, Asai Y, Kamiyoshi K, Watanabe T, Kawaoka Y, Kitano H. systemsDock: a web server for network pharmacology-based prediction and analysis. Nucleic Acids Res 2016;44:W507–13. https://doi.org/10.1093/NAR/GKW335.
[58] Tabrez S, Rahman F, Ali R, Muhammad F, Alshehri BM, Alaidarous MA, Banawas S, Bin Dukhyil AA, Rub A. Repurposing of FDA-approved drugs as inhibitors of sterol C-24 methyltransferase of Leishmania donovani to fight against leishmaniasis. Drug Dev Res 2021;82:1154–61. https://doi.org/10.1002/DDR.21820.
[59] Martín-Martínez M, Pérez-Gordillo FL, Álvarez de La Rosa D, Rodríguez Y, Gerona-Navarro G, González-Muñiz R, Zhou MM. Modulating mineralocorticoid receptor with non-steroidal antagonists. New opportunities for the development of potent and selective ligands without off-target side effects. J Med Chem 2017;60:2629–50. https://doi.org/10.1021/ACS.JMEDCHEM.6B01065.
[60] Bramlage P, Swift SL, Thoenes M, Minguet J, Ferrero C, Schmieder RE. Non-steroidal mineralocorticoid receptor antagonism for the treatment of cardiovascular and renal disease. Eur J Heart Fail 2016;18:28–37. https://doi.org/10.1002/EJHF.444.
[61] Ertl P, Schuffenhauer A. Estimation of synthetic accessibility score of drug-like molecules based on molecular complexity and fragment contributions. J Cheminf 2009;1:1–11. https://doi.org/10.1186/1758-2946-1-8/TABLES/1.
[62] Speck-Planche A, Kleandrova VV, Luan F, Cordeiro M Natalia DS. Silico discovery and virtual screening of multi-target inhibitors for proteins in Mycobacterium tuberculosis. Comb Chem High Throughput Screen 2012;15:666–73. https://doi.org/10.2174/138620712802650487.
[63] Gupta Y, Maciorowski D, Zak SE, Jones KA, Kathayat RS, Azizi SA, Mathur R, Pearce CM, Ilc DJ, Husein H, Herbert AS, Bharti A, Rathi B, Durvasula R, Becker DP, Dickinson BC, Dye JM, Kempaiah P. Bisindolylmaleimide IX: a novel anti-SARS-CoV2 agent targeting viral main protease 3CLpro demonstrated by virtual screening pipeline and in-vitro validation assays. Methods 2021;195:57–71. https://doi.org/10.1016/j.ymeth.2021.01.003.
[64] Sidhu KS, Bhangu SK, Pathak RK, Yadav IS, Chhuneja P. Identification of natural lead compounds for leaf rust of Wheat: a molecular docking and simulation study. J Protein Proteonomics 2020;11:283–95. https://doi.org/10.1007/s42485-020-00048-5.
[65] Agyapong O, Asiedu SO, Kwofie SK, Miller WA, Parry CS, Sowah RA, Wilson MD. Molecular modelling and de novo fragment-based design of potential inhibitors of beta-tubulin gene of Necator americanus from natural products. Inform Med Unlocked 2021;26:100734/1-100734/20. https://doi.org/10.1016/j.imu.2021.100734.
[66] Broni E, Kwofie SK, Asiedu SO, Miller WA, Wilson MD. A molecular modeling approach to identify potential antileishmanial compounds against the cell division cycle (cdc)-2-Related kinase 12 (CRK12) receptor of leishmania donovani. Biomolecules 2021;11:458/1-458/32. https://doi.org/10.3390/biom11030458.
[67] Pathania S, Singh PK, Narang RK, Rawal RK. Identifying novel putative ERK1/2 inhibitors via hybrid scaffold hopping –FBDD approach. J Biomol Struct Dyn 2021;39:1–16. https://doi.org/10.1080/07391102.2021.1889670.
[68] Dunn MF. Protein–ligand interactions: general description. ELS; 2010. p. 1–12. https://doi.org/10.1002/9780470015902.a0001340.pub2.
[69] Ikwu FA, Isyaku Y, Obadawo BS, Lawal HA, Ajibowu SA. In silico design and molecular docking study of CDK2 inhibitors with potent cytotoxic activity against HCT116 colorectal cancer cell line. J Genet Eng Biotechnol 2020;18:1–12. https://doi.org/10.1186/s43141-020-00066-2.
[70] Harel D, Khalid SA, Kaiser M, Brun R, Wünsch B, Schmidt TJ. Encecalol angelate, an unstable chromene from Ageratum conyzoides L.: total synthesis and investigation of its antiprotozoal activity. J Ethnopharmacol 2011;137:620–5. https://doi.org/10.1016/j.jep.2011.06.015.
[71] Arango V, Robledo S, Séon-Méniel B, Figadère B, Cardona W, Sáez J, Otálvaro F. Coumarins from Galipea panamensis and their activity against Leishmania panamensis. J Nat Prod 2010;73:1012–4. https://doi.org/10.1021/NP100146Y.
[72] Kwofie S, Broni E, Yunus F, Nsoh J, Adoboe D, Miller W, Wilson M. Molecular docking simulation studies identifies potential natural product derived-antiwolbachial compounds as filaricides against onchocerciasis. Biomedicines 2021;9:1682/1-1682/33. https://doi.org/10.3390/biomedicines9111682.
[73] Lipinski CA. Lead- and drug-like compounds: the rule-of-five revolution. Drug Discov Today Technol 2004;1:337–41. https://doi.org/10.1016/J.DDTEC.2004.11.007.
[74] Kwofie SK, Annan DG, Adinortey CA, Boison D, Kwarko GB, Abban RA, Adinortey MB. Identification of novel potential inhibitors of varicella-zoster virus thymidine kinase from ethnopharmacologic relevant plants through an in-silico approach. J Biomol Struct Dyn 2021:1–17. https://doi.org/10.1080/07391102.2021.1977700.
[75] Ntie-Kang F, Zofou D, Babiaka SB, Meudom R, Scharfe M, Lifongo LL, Mbah JA, Mbaze LMa, Sippl W, Efange SMN. AfroDb: a select highly potent and diverse natural product library from African medicinal plants. PLoS One 2013;8:e78085/1-e78085/15. https://doi.org/10.1371/JOURNAL.PONE.0078085.
[76] Kwofie SK, Broni E, Asiedu SO, Kwarko GB, Dankwa B, Enninful KS, Tiburu EK, Wilson MD. Cheminformatics-based identification of potential novel anti-sars-cov-2 natural compounds of african origin. Molecules 2021;26:1–35. https://doi.org/10.3390/molecules26020406.
[77] Veber DF, Johnson SR, Cheng HY, Smith BR, Ward KW, Kopple KD. Molecular properties that influence the oral bioavailability of drug candidates. J Med Chem 2002;45:2615–23. https://doi.org/10.1021/JM020017N.
[78] van den Anker J, Reed MD, Allegaert K, Kearns GL. Developmental changes in pharmacokinetics and pharmacodynamics. J Clin Pharmacol 2018;58:S10–25. https://doi.org/10.1002/JCPH.1284.
[79] Sawale RT, Kalyankar TM, George R, Deosarkar SD. Molar refraction and polarizability of antiemetic drug 4-amino-5-chloro-N-(2-(diethylamino)ethyl)-2 methoxybenzamide hydrochloride monohydrate in {Aqueous-Sodium or lithium chloride} solutions at 30 o C. J Appl Pharmaceut Sci 2016;6:120–4. https://doi.org/10.7324/JAPS.2016.60321.
[80] Flores-Sumoza M, Alcázar JJ, Márquez E, Mora JR, Lezama J, Puello E. Classical QSAR and docking simulation of 4-pyridone derivatives for their antimalarial activity. Mol 2018;23:3166/1-3166/12. https://doi.org/10.3390/MOLECULES23123166. Page 3166. 23 (2018).
[81] Ertl P, Schuffenhauer A. Estimation of synthetic accessibility score of drug-like molecules based on molecular complexity and fragment contributions. J Cheminf 2009;1:1–11. https://doi.org/10.1186/1758-2946-1-8/TABLES/1.
[82] Alavijeh MS, Chishty M, Qaiser MZ, Palmer AM. Drug metabolism and pharmacokinetics, the blood-brain barrier, and central nervous system drug discovery. NeuroRx 2005;2:554–71. https://doi.org/10.1602/NEURORX.2.4.554.

[83] Glassman PM, Muzykantov VR. Pharmacokinetic and pharmacodynamic properties of drug delivery systems. J Pharmacol Exp Therapeut 2019;370: 570–80. https://doi.org/10.1124/JPET.119.257113.

[84] Islam MA, Pillay TS. Identification of promising anti-DNA gyrase antibacterial compounds using de novo design, molecular docking and molecular dynamics studies. J Biomol Struct Dyn 2019;38:1798–809. https://doi.org/10.1080/07391102.2019.1617785.

[85] Löbenberg R, Amidon GL, Ferraz HG, Bou-Chacra N. Mechanism of gastrointestinal drug absorption and application in therapeutic drug delivery. Ther Deliv Methods A Concise Overv Emerg Areas 2013:8–22. https://doi.org/10.4155/EBO.13.349/ASSET/IMAGES/LARGE/FIGURE6. JPEG.

[86] Suenderhauf C, Hammann F, Huwyler J. Computational prediction of blood-brain barrier permeability using decision tree induction. Molecules 2012;17:10429–45. https://doi.org/10.3390/MOLECULES170910429.

[87] Broni E, Kwofie SK, Asiedu SO, Miller WA, Wilson MD. A molecular modeling approach to identify potential antileishmanial compounds against the cell division cycle (Cdc)-2-related kinase 12 (crk12) receptor of leishmania donovani. Biomolecules 2021;11:458/1-458/32. https://doi.org/10.3390/biom11030458.

[88] Lin JH, Yamazaki M. Role of P-glycoprotein in pharmacokinetics: clinical implications. Clin Pharmacokinet 2003;42:59–98. https://doi.org/10.2165/00003088-200342010-00003.

[89] Parasuraman S. Prediction of activity spectra for substances. J Pharmacol Pharmacother 2011;2:52–3. https://doi.org/10.4103/0976-500X.77119.

[90] Stepanchikova A, Lagunin A, Filimonov D, Poroikov V. Prediction of biological activity spectra for substances: evaluation on the diverse sets of drug-like structures. Curr Med Chem 2012;10:225–33. https://doi.org/10.2174/0929867033368510.

[91] Perez J, Fuertes M, Nguewa P, Castilla J, Alonso C. Anticancer compounds as leishmanicidal drugs: challenges in chemotherapy and future perspectives. Curr Med Chem 2008;15:433–9. https://doi.org/10.2174/092986708783503221.

[92] Sanderson L, Yardley V, Croft SL. Activity of anti-cancer protein kinase inhibitors against Leishmania spp. J Antimicrob Chemother 2014;69:1888–91. https://doi.org/10.1093/JAC/DKU069.

[93] Kalmi G, Vignon-Pennamen MD, Ram-Wolff C, Battistella M, Lafaurie M, Bouaziz JD, Hamane S, Bernard S, Bretagne S, Thiéblemont C, Bagot M, de Masson A. Visceral leishmaniasis in patients with lymphoma: case reports and review of the literature. Medicine (Baltimore) 2020;99:e22787/1-e22787/5. https://doi.org/10.1097/MD.0000000000022787.

[94] Machado PRL, Ribeiro CS, França-Costa J, Dourado MEF, Trinconi CT, Yokoyama-Yasunaka JKU, Malta-Santos H, Borges VM, Carvalho EM, Uliana SRB. Tamoxifen and meglumine antimoniate combined therapy in cutaneous leishmaniasis patients: a randomised trial. Trop Med Int Health 2018;23:936–42. https://doi.org/10.1111/TMI.13119.

[95] Pulivarthi D, Steinberg KM, Monzote L, Piñón A, Setzer WN. Antileishmanial activity of compounds isolated from sassafras albidum. Nat Prod Commun 2015; 10:1229–30. https://doi.org/10.1177/1934578X1501000723.

[96] Weidner S, Kittelmann M, Goeke K, Ghisalba O, Zähner H. 3'-Demethoxy-3'-hydroxystaurosporine-O-methyltransferase from Streptomyces longisporoflavus catalyzing the last step in the biosynthesis of staurosporine. J Antibiot (Tokyo) 1998;51:679–82. https://doi.org/10.7164/ANTIBIOTICS.51.679.

[97] Axelrod J, Daly J. Phenol-O-methyltransferase. BBA - Enzymol. 1968;159:472–8. https://doi.org/10.1016/0005-2744(68)90131-9.

[98] Coque JJR, Alvarez-Rodríguez ML, Larriba G. Characterization of an inducible chlorophenol O-methyltransferase from Trichoderma longibrachiatum involved in the formation of chloroanisoles and determination of its role in cork taint of wines. Appl Environ Microbiol 2003;69:5089–95. https://doi.org/10.1128/AEM.69.9.5089-5095.2003/ASSET/943B581A-42DB-4174-B2A8-9A9FE5E9C153/ASSETS/GRAPHIC/AM0930278003. JPEG.

[99] Chi Y, Gao K, Zhang H, Takeda M, Yao J. Suppression of cell membrane permeability by suramin: involvement of its inhibitory actions on connexin 43 hemichannels. Br J Pharmacol 2014;171:3448–62. https://doi.org/10.1111/BPH.12693.

[100] Sarkar P, Yarlagadda V, Ghosh C, Haldar J. A review on cell wall synthesis inhibitors with an emphasis on glycopeptide antibiotics. Medchemcomm 2017;8: 516–33. https://doi.org/10.1039/C6MD00585C.

[101] Poole K. Bacterial stress responses as determinants of antimicrobial resistance. J Antimicrob Chemother 2012;67:2069–89. https://doi.org/10.1093/JAC/DKS196.

[102] Singh VS, Dhawale SC, Shakeel F, Faiyazuddin M, Alshehri S. Antiarthritic potential of calotropis procera leaf fractions in FCA-induced arthritic rats: involvement of cellular inflammatory mediators and other biomarkers. Agriculture 2021;11:68–84. https://doi.org/10.3390/AGRICULTURE11010068.

[103] Hossen MA, Reza ASMA, Ahmed AMA, Islam MK, Jahan I, Hossain R, Khan MF, Maruf MRA, Haque MA, Rahman MA. Pretreatment of Blumea lacera leaves ameliorate acute ulcer and oxidative stress in ethanol-induced Long-Evan rat: a combined experimental and chemico-biological interaction. Biomed Pharmacother 2021;135:111211/1-111211/11. https://doi.org/10.1016/J.BIOPHA.2020.111211.

[104] Adeola Falade V, Isaac Adelusi T, Olaide Adedotun I, Abdul-Hammed M, Alabi Lawal T, Alabi Agboluaje S, Silico I. Pharmacology, in silico investigation of saponins and tannins as potential inhibitors of SARS-CoV-2 main protease (Mpro). Silico Pharmacol 2021;9:1–15. https://doi.org/10.1007/S40203-020-00071-W.

[105] Zhang G, Guo K, Wang P, Shan Y, Ma C. Identification of the new in vivo metabolites of ilaprazole in rat plasma after oral administration by LC-MS: in silico prediction of the H+/K+-ATPase inhibitor. Molecules 2021;26:459–76. https://doi.org/10.3390/MOLECULES26020459.

[106] Gervazoni LFO, Barcellos GB, Ferreira-Paes T, Almeida-Amaral EE. Use of natural products in leishmaniasis chemotherapy: an overview. Front Chem 2020;8:1031/1-1031/43. https://doi.org/10.3389/FCHEM.2020.579891/BIBTEX.

[107] Baloch N, Alkahraman YMSA, Zaidi MA, Madkour HMF. Evaluation of 6, 8-Dichloro-2-methyl-4H-Chromen-4-one derivatives as antileishmanial agents. Glob J Sci Front Res (GJSFR) 2012;12:2–8.

[108] Song C-H, Kim N, Kim D-H, Lee H-N, Surh Y-J. 17-β estradiol exerts anti-inflammatory effects through activation of Nrf2 in mouse embryonic fibroblasts. PLoS One 2019;14:e0221650/1-e0221650/13. https://doi.org/10.1371/journal.pone.0221650.

[109] Wu X, Zhang S, Zhang Q, Zhao Y, Chen G, Guo W, Wang L. The contribution of specific subsites to catalytic activities in active site architecture of a GH11 xylanase. Appl Microbiol Biotechnol 2020;104:8735–45. https://doi.org/10.1007/S00253-020-10865-9.

[110] Azam SS, Abro A, Raza S, Saroosh A. Structure and dynamics studies of sterol 24-C-methyltransferase with mechanism based inactivators for the disruption of ergosterol biosynthesis. Mol Biol Rep 2014;41:4279–93. https://doi.org/10.1007/S11033-014-3299-Y.

[111] Asiedu SO, Kwofie SK, Broni E, Wilson MD. Computational identification of potential anti-inflammatory natural compounds targeting the p38 mitogen-activated protein kinase (MAPK): implications for COVID-19-induced cytokine storm. Biomolecules 2021;11:653–78. https://doi.org/10.3390/BIOM11050653.

[112] Congreve M, Marshall F. The impact of GPCR structures on pharmacology and structure-based drug design. Br J Pharmacol 2010;159:986–96. https://doi.org/10.1111/J.1476-5381.2009.00476.X.

[113] Grinter SZ, Zou X. Challenges, applications, and recent advances of protein-ligand docking in structure-based drug design. Molecules 2014;19:10150–76. https://doi.org/10.3390/MOLECULES190710150.

[114] Bronowska AK. Thermodynamics - interaction studies - Solids, liquids and gases. Thermodyn. - Interact. Stud. - Solids, Liq. Gases 2011:1–49. https://doi.org/10.5772/823.

[115] Estrada E, Uriarte E, Vilar S. Effect of protein backbone folding on the stability of protein-ligand complexes. J Proteome Res 2006;5:105–11. https://doi.org/10.1021/pr0503174.

[116] Kwofie S, Dankwa B, Enninful K, Adobor C, Broni E, Ntiamoah A, Wilson M. Molecular docking and dynamics simulation studies predict Munc18b as a target of mycolactone: a plausible mechanism for granule exocytosis impairment in buruli ulcer pathogenesis. Toxins (Basel) 2019;11:181/1-181/16. https://doi.org/10.3390/toxins11030181.

[117] Skjevik ÅA, Teigen K, Martinez A. Overview of computational methods employed in early-stage drug discovery. Future Med Chem 2009;1:49–63. https://doi.org/10.4155/FMC.09.7.

[118] Mak KK, Pichika MR. Artificial intelligence in drug development: present status and future prospects. Drug Discov Today 2019;24:773–80. https://doi.org/10.1016/J.DRUDIS.2018.11.014.

[119] Bajorath J. Integration of virtual and high-throughput screening. Nat Rev Drug Discov 2002;1:882–94. https://doi.org/10.1038/NRD941.

[120] Zheng M, Zhao J, Cui C, Fu Z, Li X, Liu X, Ding X, Tan X, Li F, Luo X, Chen K, Jiang H. Computational chemical biology and drug design: facilitating protein structure, function, and modulation studies. Med Res Rev 2018;38:914–50. https://doi.org/10.1002/MED.21483.

[121] Riolo G, Cantara S, Marzocchi C, Ricci C. miRNA targets: from prediction tools to experimental validation. Methods Protoc 2020;4:1–20. https://doi.org/10.3390/MPS4010001.

[122] Mateus A, Määttä TA, Savitski MM. Thermal proteome profiling: unbiased assessment of protein state through heat-induced stability changes. Proteome Sci 2017;15:e9232/1-e9232/11. https://doi.org/10.1186/S12953-017-0122-4.

[123] Das A, Das MC, Das N, Bhattacharjee S. Evaluation of the antileishmanial potency, toxicity and phytochemical constituents of methanol bark extract of Sterculia villosa. Pharm Biol 2017;55:998–1009. https://doi.org/10.1080/13880209.2017.1285946.

[124] Silva J de C, de França PRL, Converti A, Porto TS. Kinetic and thermodynamic characterization of a novel Aspergillus aculeatus URM4953 polygalacturonase. Comparison of free and calcium alginate-immobilized enzyme. Process Biochem 2018;74:61–70. https://doi.org/10.1016/J.PROCBIO.2018.07.010.

[125] Baig MH, Ahmad K, Rabbani G, Danishuddin M, Choi I. Computer aided drug design and its application to the development of potential drugs for neurodegenerative disorders. Curr Neuropharmacol 2018;16:740–8. https://doi.org/10.2174/1570159X15666171016163510.

[126] Talele T, Khedkar S, Rigby A. Successful applications of computer aided drug discovery: moving drugs from concept to the clinic. Curr Top Med Chem 2010;10: 127–41. https://doi.org/10.2174/156802610790232251.

[127] Ganeshpurkar A, Saluja AK. The pharmacological potential of rutin. Saudi Pharmaceut J 2017;25:149–64. https://doi.org/10.1016/j.jsps.2016.04.025.

[128] Kant V, Ranjan R, Kumar P, Mandal D, Vijayakumar S. Silico screening , molecular dynamic simulations , and in vitro activity of selected natural compounds as an inhibitor of Leishmania donovani 3 - mercaptopyruvate sulfurtransferase. Parasitol Res 2022:2093. https://doi.org/10.1007/s00436-022-07532-5. –2109.